Aalto-yliopisto
Insinööritieteiden
korkeakoulu

Teemu Routa

Finite difference method in assessment of suitable mining method to Kemi mine

Master's thesis that has been left to be inspected for the degree of Master of Science

Espoo 21.02.2021
Supervisor: Professor Mikael Rinne
Advisors: M. Sc. Harri Kuula
M. Sc. Mikko Lamberg

Aalto University
School of Engineering

Aalto University, P.O. BOX 11000, 00076 AALTO
www.aalto.fi

Abstract of master's thesis

Author Teemu Routa

Title of thesis Finite difference method in assessment of suitable mining method in Kemi mine

Master program Geoengineering **Code** ENG23

Thesis supervisor Mikael Rinne

Thesis advisor(s) Harri Kuula, Mikko Lamberg

Date 21.2.2021 **Number of pages** 59+5 **Language** English

Abstract

Kemi mine will soon begin excavations from the new underground mine expansion, reaching the depth of-1500 meters. Kemi mine wants to increase efficiency of ore excavation and has conducted studies to find out whether current mining method could be changed to cave mining. This thesis aim was to study the effects of sub level caving mining would create to mine in large scale. The study was done using Fast Lagrangian Analysis of Continua in 3 Dimensions software in large strain mode.

Simulation model was made to include different rock types in the Kemi mine's geological environment and weakness zones. Kemi mine has conducted many rock mechanical analyses of the the Kemi mine in past. This cumulative knowledge was used in model geometry creation and determination of different rock types mechanical properties for simulation parameters. This was used as base point to calibrate simulation model to as close to real state of the mine as was reasonable possible.

Once the simulated current state of the mine corresponded well with the real displacements and failures at the ground surface, different mining scenarios were simulated. One of the scenarios were a reference scenario in where the new underground mine expansion was mined with the current mining method.

For the other mining scenarios containing varying amounts of sub level caving-mining, a new sub level caving-simulation logic was created. This new simulation logic was used to simulate the overall effects of the sub level caving-mining to the Kemi mine.

Most of the results are mainly indicative in nature due the lack of verification of new sub level caving-mining simulation logic. Yet as the results are reasonable in direction-, scale- and area wise, some interesting observations can be made.

Keywords 3D-simulation, Sub-level-caving, rock mechanics, underground-benching with backfill

Aalto-yliopisto
Insinööritieteiden
korkeakoulu

Aalto-yliopisto, PL 11000, 00076 AALTO
www.aalto.fi

Diplomityön tiivistelmä

Tekijä Teemu Routa

Työn nimi Finite difference-menetelmän käyttö sopivan louhintamenetelmän arvoinnissa Kemin kaivokseen

Koulutusohjelma Geoengineering **Koodi** ENG23

Vastuuopettaja/valvoja Mikael Rinne

Työn ohjaaja(t) Harri Kuula, Mikko Lamberg

Päivämäärä 21.2.2021 **Sivumäärä** 59+5 **Kieli** English

Tiivistelmä

Kemin maanalaista kaivosta on laajennettu ja syvimmät louhokset ylettyvät -1500 tasolle asti. Malmin louhinnan tehostamiseksi Kemin kaivos on tilannut useita selvityksiä siitä että, voisiko nykyistä louhintamenetelmää vaihtaa sorroslouhinta menetelmään. Tämän diplomityön tarkoituksena on tutkia, mitä vaikutuksia louhintamenetelmän vaihtaminen levysorroslouhintaan aiheuttaisi kaivokselle koko kaivoksen mittakaavassa. Tutkimus tehtiin Fast Lagrangian Analysis of Continua in 3 Dimensions-simulointiohjelmalla.

Simulaatiomalliin sisällytettiin Kemin kaivoksen alueella olevia eri kivilajeja ja heikkousvyöhykkeitä. Kemin kaivos on tilannut useita kalliomekaanisia simulointeja Kemin kaivoksesta. Tässä työssä on hyödynnetty aiempien kalliomekaanisten simulaatioiden tietoa simulaatiomallin rakentamisessa ja eri kivilajien simulaatioparametrien määrittämisessä. Tätä käytettiin työssä pohjana simulaatiomallin kalibrointiin, jotta malli vastaisi todellisuutta mahdollisimman hyvin.

Kun simulaatiomallin tulokset kaivoksen nykyisestä tilasta vastasivat hyvin maanpäällä havaituista siirtymistä- ja murtumista, alkoi eri simulaatioskenaarioden simulointi. Yksi skenaarioista oli vertailu skenaario, jossa uusi maanalainen laajennus louhittaisiin kokonaan nykyisellä louhintamenetelmällä.

Toiset louhintaskenaariot sisälsivät vaihtelevan verran levysorroslouhintaa. Tämän louhintamenetelmän vaikutusten simulointia varten tässä työssä kehitettiin uusi simulaatiologiikka. Useat työn tulokset ovat suuntaa antavia uuden simulaatiologiikan takia. Työssä kehitettyä uutta simulaatiologiikkaa Levysorroslouhinnan vaikutusten simulointiin ei ole vielä verifioitu. Tästä huolimatta tulokset ovat järkeviä suuntansa, mittakaavansa, ja laajuutensa puolesta, mikä mahdollistaa mielenkiintoisten havaintojen tekemisen.

Avainsanat 3D-simulointi, levysorroslouhinta, kalliomekaniikka, pengerlouhinta

Preface

Outokumpu Oy has ordered many rock mechanical simulations from AFRY Finland Oy (former Pöyry Finland Oy) during operation time. One of the rock mechanical simulation task was agreed to conduct as an master's thesis. This is an in depended study that was ordered by Outokumpu Oy from AFRY Finland Oy and carried out by me.

From Outokumpu Oy Jaakko Ihanus, Markus Karlsson and Timo Nikkinen participated to thesis the guiding team. Other participant were my advisors from AFRY Finland Oy Harri Kuula and Mikko Lamberg and my thesis supervisor professor Mikael Rinne from the Aalto University school of Engineering.

Purpose of the thesis was to study mining induced affects caused by different mining methods and combinations of them. Funding for the thesis was arranged between Outokumpu Oy, AFRY Finland Oy and me in a way, that AFRY Finland Oy invoiced 600 hours of the my working time from Outokumpu Oy and I was paid the same amount of working hours by AFRY Finland Oy as an hourly based salary.

I want to thank Outokumpu Oy and AFRY Finland Oy of the opportunity to challenge myself and deepen my knowledge on rock mechanical simulations. I also want to thank whole heartily my whole thesis guiding team of the high quality guidance I received, Luca Broda from AFRY Finland Oy of the technical- and expertise to support of used software, fellow co-workers at AFRY Finland Oy as well as my Family and live-in partner of the emotional support they have given throughout my time with the thesis.

Espoo 21.2.2021

Teemu Routa

Contents

Symbols

$A_{Caved\ rocks}$	[m^2]	Area of excavation induced loose rocks
$A_{Caving\ area}$	[m^2]	Area of excavation induced caving
$A_{Average\ mining\ level}$	[m2]	Area of average mining level
D	[]	Rock disturbance factor
E_i	[MPa]	Deformation modulus for intact rock
E_{rm}	[MPa]	Deformation modulus for rock mass
G	[MPa]	D shear modulus for the rock mass
GSI_r	[]	Geological strength index residual value
H_P	[m]	Depth of interpretation point
H_{P1}	[m]	Depth of interpretation point 1
H_{P2}	[m]	Depth of interpretation point 2
J_a	[]	Joint alteration number
J_n	[]	Joint set number
J_r	[]	Joint roughness number
J_w	[]	Joint Water Reduction Factor
K	[GPa]	Bulk modulus for the rock mass
$N_{levels\ of\ rock\ support}$	[]	Number of levels of caved rocks provides support
L	[m]	Length of the drill core
Q	[]	NQI system value
a	[]	Rock mass quality parameter
a_r	[]	Residual value of a
c	[MPa]	Cohesion
c'	[MPa]	Cohesion from Hoek-Brown to Mohr-coulomb calculation
m_b	[]	Reduced constant of m_i
m_i	[]	Intact rock quality parameter
m_r	[]	Residual value of m_i
s	[]	Rock mass quality parameter
s_r	[]	Residual value of s
v	[]	Poisson's ratio
x_i	[m]	Length of piece of 0,1 m or longer within drill core
α	[°]	Angle from model's x-axis (from north)
β	[°]	Angle from model's y-axis (from north)
σ_{ci}	[MPa]	Uniaxial compressive strength for intact rock
Δz	[m]	Length of the zone's edge
$\in_{crit}^{ps}$	[]	Critical plastic strain
σ_{tm}	[MPa]	Rock masses tensile strength
σ_x	[MPa]	Component in x-direction of stress gradients in Z--direction.
σ_y	[MPa]	Component in y-direction of stress gradients in Z--direction.
σ_1	[MPa]	Major principal stress magnitude
σ_{1ip}	[MPa]	Major principal stress at interpretation point
σ_3	[MPa]	Minor principal stress magnitude
σ_{3ip}	[MPa]	Minor principal stress at interpretation point

σ'_{3max}	[MPa]	Maximum value of σ'_3 for equivalent Hoek-Brown and Mohr-Coulomb
σ_{iP0}	[MPa]	Axial stress at base point (0,0,0)
σ_{iP}	[MPa]	Axial stress i at interpretation point
$\sigma_{i\Delta Z}$	[MPa]	Axial stress gradient
$\sigma_{i\Delta Z}$	[MPa]	Axial stress gradient
σ_{iP1}	[MPa]	Axial stress i at interpretation point 1
σ_{iP2}	[MPa]	Axial stress i at interpretation point 2
φ	[°]	Friction angle
φ'	[°]	Friction angle from Hoek-Brown to Mohr-coulomb calculation

Abbreviations

Deep I	Deep mine mining levels -500 to -1000
Deep II	Deep mine mining levels -1000 to -1500
EL	Elijärvi
ELPV	Elijärvi Pohjois-Viia open pit
FLAC3D	Fast Lagrangian Analysis of Continua in 3 Dimensions
GR	Granite
GSI	Geological strength index
IV	Itä-Viia
LV	Länsi-Viia
MO	Mätäsoja
MPRD	Metamorphic periodate
MPYR	Metamorphic pyroxenite
NJ	Nuottijärvi
ORE	Orebody
PV	Pohjois-Viia
RQD	Rock Quality Designation
SLC	Sub level caving
SO	Surmaoja
S0	Simulation scenario 0
S1	Simulation scenario 1
S2	Simulation scenario 2
S3	Simulation scenario 3
TLKKRB	Talc-carbonite
UCS	Uniaxial compression strength
UGB	Underground benching
VP	Viianmaa-Perukka

1 Introduction and problem description

Kemi mine is owned by Outokumpu Oy. The Kemi mine is the largest underground mine in Finland and its annual production capacity of ore is around 2,7 million tons. The mined ore from the Kemi mine is chrome. Kemi mine is the only chrome mine within European Union's area. (Salmi 2018).

Kemi mine's ore deposit was discovered in 1959. The mine was opened during the year 1968. The mining started as an open pit mine and continued to the depth of 200 meters. The Ending depth of open pit mining was achieved after 41 years of mining in 2005. (Salmi 2018).

Underground mining was started two years before the open pit mining was finished in 2003. The infrastructure for underground mining has been built to the footwall side, which is mainly hard granite. Underground mining started from level 550 and continued upwards towards bottom of the crown pillar on level 275 (Rikberg 2019). Currently Outokumpu is expanding the underground mine to the level 1000, where new main level and drift is being built.

Outokumpu has considered of switching the used mining method to mine the chromite ore more efficiently. Before switching the used mining method within Kemi mine, Outokumpu Oy wants to compare the effects from continuation of current- and switching to new mining method will have for the stability of the whole mine.

The underground mining in the Kemi mine have done using underground benching with fill or in short UGB. Outokumpu has considered of using sub level caving or in short SLC method for mining in future. Finite difference method were chosen by Outokumpu Oy and AFRY Oy to be the method of simulation of different mining scenarios. In this thesis the used finite difference method software is ITASCA Consulting Group Inc.'s Fast Lagrangian Analysis of Continua in 3 Dimensions, in short FLAC3D.

The research material will consist of scientific books, -articles and guides. Additionally, material given by AFRY Finland and Outokumpu will be used. This additional data will include: geological interpretation of the Kemi mine, earlier stability model from underground benching with fill simulations and other documents relevant to the thesis. The used research methods are:

- Literature review
- Modelling and stability simulation with FLAC3D
- The comparison of the results from the different simulations.

1.1 Research questions, objective and scope

For the Outokumpu Oy mine's global stability is absolutely crucial factor in selection of the used mining method. As such the chosen main research question of the thesis is; how the different mining methods would affect the Kemi mine's global stability. In addition of global stability of the mine, Outokumpu Oy is interested in mining induced surface displacements, combination of UGB- and SLC-mining. Thus additional research questions for the thesis are:

- How would SLC mining affect the ground surface around the mining area and to the fixed installations to the footwall side on the ground surface?
- How would combinations of partially UGB- and SLC mining affect the mine's stability?
- How the simulation model can be made to represent the effects of the SLC mining?

The objective of this master thesis is to produce a research that helps Outokumpu in assessment of feasibility of different mining methods. This is achieved by studying the effects of UGB- and SLC mining cause to the surrounding rock mass and open spaces using numerical method FLAC3D. The effects of the mining are studied by examining the development of:

- Displacements, in addition to magnitude of the displacement, the displacements in Z-direction in the model are examined. These two directions correspond to the most crucial direction in relation to the excavated ore body: Y-axis to mine's underground infrastructure and Z-axis to surface displacements. X-axis of model is less important as it is parallel to the orebodies and thus only very small displacements are noticed.
- Total strain increment is used to represent large cracks on surface.
- Plastic strain increment, for highlighting areas that have yielded irreversibly.
- Velocity is used to examine whether any significant movements occur within model during significant amount of steps. This is used to evaluate if the model has reached state sufficiently close to equilibrium.

As the focus of the thesis is to study the Outokumpu Oy's chosen mining methods and those methods effect on the mine's global stability, it is necessary to exclude intriguing elements from the study. Otherwise the scope of the thesis would be too wide, thus the time schedule and the required calculation resources would stretch to unacceptable limits. All the other mining methods other than UGB with backfill, SLC and combination of these are excluded from the study.

The focus of the simulations is to study the global stability and the displacements in mine's vicinity. As such there is no need to assign resources to simulate the exact SLC-behavior within mining stopes and -levels. Instead of accurate simulation of rock flow within the excavation area, assumptions are made to simplify the model and simulations. The details of used assumptions are discussed in the chapter 4.5.1.

2 Rock mechanic theory for simulations

In this chapter is represented the needed theoretical background for modelling of the rock mass classification, caving mechanisms and used failure criterions in thesis.

2.1 Rock mass characteristics, -classification and caving

Rock mass consists of intact rock material and structural discontinuities such as: joints and faults. Rock structure refers to the combination of different structural discontinues and distribution of them (Brady & Brown 2005). Rock structure is important factor for classifying rock masses.

According Brady & Brown (2005) major structural features of rock mass are: bedding planes, folds, faults, shear zones, dykes, joints and veins. Among the major structural features in rock mass, joints are very common and have considerable effect on mechanical properties of rock mass. Joints are discontinuities within rock mass, where visible displacement can't be observed. Parallel joints are joint sets and joint sets that intersect each other are called joint system. Joint orientation is often represented using dip and - direction. Dip is the joint's declination from horizontal and dip direction is the angle measured from true north.

Rock mass's intactness can be/ may classified by using Rock Quality Designation (RQD) values. RQD quantifies the spacing of the discontinuities within the rock mass (Brady & Brown 2005). RQD-values vary from 0 to 100. Rock mass with RQD-value of 0 is very jointed and with value of 100 not jointed or only slightly jointed. RQD values are calculated often from drill cores using equation:

$$RQD = \frac{100 \sum x_i}{L} \quad (1)$$

where x_i is the length of piece of 0,1 m or longer within the drill core
L is the length of the drill core

A more accurate classification system is the Barton et. al.'s the NQI Q system. The Q system takes into consideration rock mass's intactness using RQD values, joint characteristics and stress (Brady & Brown 2005). It is widely used in practical rock engineering. The Q value range on logarithmic scale from 000.1 to 1000 and is calculated as:

$$Q = \left(\frac{RQD}{J_n}\right) * \left(\frac{J_r}{a}\right) * \left(\frac{J_w}{SRF}\right) \quad (2)$$

where RQD is the Rock Quality Designation-value from the equation 1
J_n is the Joint set number
J_r is the Joint roughness number
J_a is the Joint alteration number
J_w is the Joint Water Reduction Factor
SRF is the Stress Reduction Factor

An another widely used rock mass classification method is the Geological strength index (GSI). The GSI takes into account the rock mass's discontinuities to the strength and deformability by evaluating the structure of the rock mass and the properties of the discontinuity surfaces. (Brady & Brown 2005).

Brady & Brown (2005) discussed that rock mass breaks by fracturing and that fracturing can occur from brittle fracture with strain-softening to ductile deformation. In Brittle fracture the rock mass's strength degreases drastically after the peak strength is achieved. The post-peak behavior depends on the softening or hardening properties of the rock mass. The stress-strain curve shapes of the post-peak behaviors are illustrated in the Figure 1.

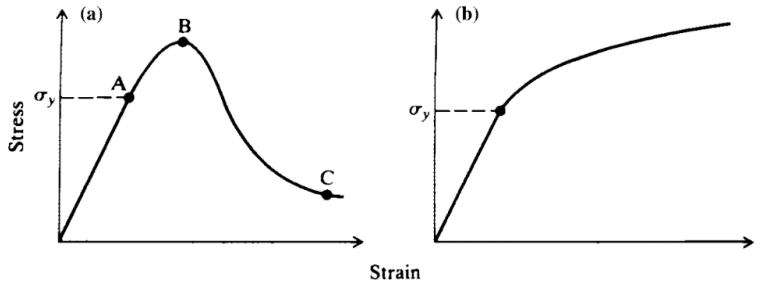

Figure 1 Post-peak stress-strain curves: a) strain-softening and b) strain-hardening by Brady & Brown (2005)

Caving occurs when cave propagates without external forces. The two main components for caving are stress and gravity. Caving can be induced by either stress or gravity. In stress induced caving stresses in the rock mass around cave exceed the strength of the rock mass. This causes the rock mass to deform and fragment into a caved material. The gravity driven caving occurs by tensile driven failure in the upper parts of the cave. (Sainsbury 2012).

The Laubsher empirical method states that the states of the cave are: "no caving", "transitional" or "caving". When the cave is in the "no caving zone", there are no major failures. In the "transitional" state the cave the caving starts and propagation is not self-sustained (Sainsbury 2012). When the cave's state is "caving", the cave propagation is self-sustained.

Main factors for cave propagation are described shortly below: (Sainsbury 2012).

1) Cohesion and tension weakening due stress and gravity. During caving the rock mass transitions from peak strength to the residual strength. This is stress-strain behavior is same as in strain-softening.
2) Post peak brittleness of the rock mass. Typically ductile rock masses wont cave as easily as brittle rock masses.
3) Reduce in deformation modulus during caving. The deformation modulus of the rock degreases as the rock mass bulks due the mobilization and yielding. As the rock mass bulks, the stress carrying capacity degreases. This has significant impact on stress redistribution around caving material.
4) Dilation behavior of the rock mass. As the rock mass dilates due shear movement, the rock mass's density changes. This impacts heavily on bulking and air gap development within caving area.

5) Discontinuities within rock mass. The rock structure has influence to caving initiation, propagation and draw angle. Faults with high dip can cut the caving geometry short and fault connecting to the ground surface can enlarge the cratering.
6) Draw plan for production area. The cave propagation and -geometry is influenced by draw rate, -position within cave and the shape of the undercut. Sainsbury mentioned that center focused withdraw may cause the cave back to arch more.
7) Pre-existence excavations. Adjacent – or excavations above of the propagating cave can have considerable effect on induced stresses around caving. For example excavation above cave can increase caving.

Typically in cave mining a self-sustained caving is desirable state. A conceptual model was developed by Duplancic and Brady (1999). to describe self-sustained cave propagation. Model consist from four different region, the regions are: elastic-, seismogenic-, yielded- and mobilized region. Typically these regions are referred as zones eg. seismogenic zone. These zones are illustrated in the Figure 2. (Sainsbury 2012).

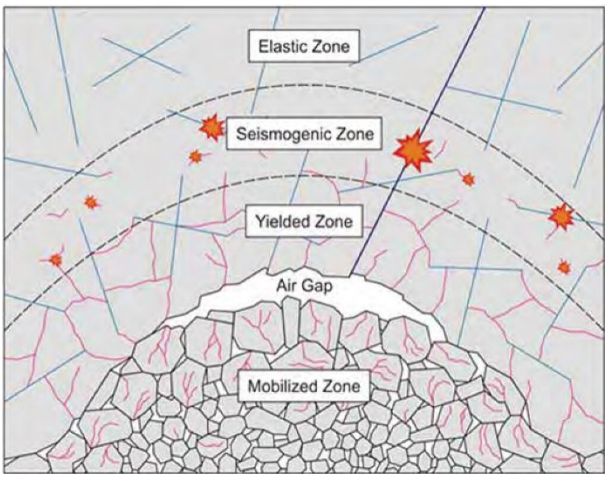

Figure 2 Propagating cave regions by Sainsbury (2012)

In the elastic zone the rock mass doesn't have major plastic deformations and can be considered as undisturbed bed rock. According Sainsbury, the seismogenic region has primary microseismic activity that is induced by small movements along existing discontinuities. Or when new fractures are being initiated.

Yielded zone has practically no cohesive strength and wont bear the overlying rock mass's weight or stresses. Due the loss of cohesive strength and the hanging nature of the yielded zone, stress magnitudes are low within it. The rock block size can reduce by either stresses or gravity. (Sainsbury 2012).

Rock in the mobilized zone is fully fragmented rock and areas of active movement. Thus it doesn't have any tensile strength or cohesion. When examining draw's impact on caving, this zone connects the draw rate to the rock mass around the cave (Sainsbury 2012). Sainsbury (2011) wrote that mobilized zone is typically interpreted of one- to two meters of total displacements.

2.2 Used failure criterions

In practice there are two failure criterions that have been used widely. These are the Mohr-Coulomb- and the Hoek-Brown criterions. Hoek-Brown model has an nonlinear failure envelope whereas Mohr-Coulomb has an linear failure envelope. In short Hoek-Brown failure envelope is better to represent nonlinear material behavior and Mohr-Coulomb calculations are require less time than Hoek.-Brown. Thus, typically Hoek-Brown is used for jointed rock mass of interest within model and Mohr-Coulomb is used for rock mass that is assumed to have only slight deformations.

Both Hoek-Brown and Mohr-Coulomb failure criterions have received updates to represent the rock mass mechanical behavior more accurately. Also for both of them are available option to include strain-softening within calculations.

The Hoek-Brown failure criterion is usually written in relation between the major- and the minor principal effective stresses. The strength of the rock is evaluated by adjusting the uniaxial compression strength of the intact rock with the GSI, geological factor and the damage rock has accumulated. The common form of the latest Hoek-Brown failure criterion is: (Hoek & Brown 2018).

$$\sigma_1 = \sigma_3 + \sigma_{ci}\left(m_b \frac{\sigma_3}{\sigma_{ci}} + s\right)^a \tag{3}$$

where σ_1 is the major principal stress magnitude
σ_3 is the minor principal stress magnitude
m_b is reduced from constant m_i, rock mass quality parameter
σ_{ci} is the uniaxial compressive strength for intact rock (MPa)
s is rock mass quality parameter
a is rock mass quality parameter

Parameter m_b, s and a are Hoek-Brown failure envelope parameters. The parameter $m_b$is reduced geological factor of the intact rock. It represent the frictional properties of the rock mass and is calculated by using equation (5).

$$m_b = m_i e^{(GSI-100)/(28-14D)} \tag{4}$$

where m_i is the intact rock quality parameter
GSI is the Geological strength index value
D is rock disturbance factor

Cai (2010) discussed that, m_i refers to intact rock's content of minerals, texture and foliation. High quality rocks have higher values of m_i than poor quality rocks. In the Figure 3 is represented influence the m_i has to the Hoek-Brown failure envelope.

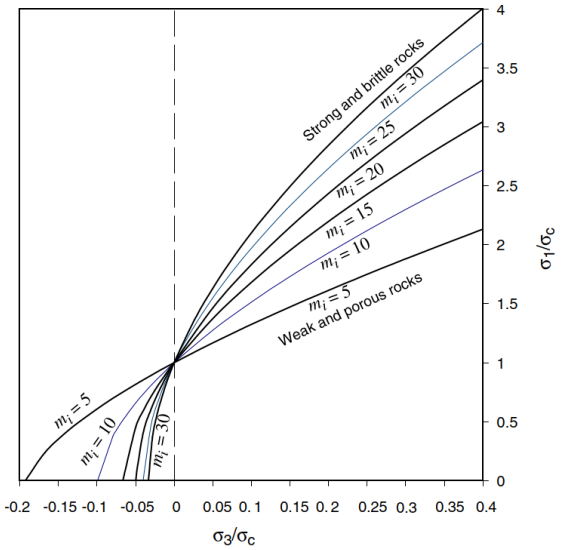

Figure 3 Hoek-Brown failure envelopes with different values of m_i by Cai (2010)

The rock disturbance factor correlates to amount of damage from excavation the rock has accumulated from excavation and stress-changes. It's values vary from the perfectly intact rock's value of 0 to the highly disturbed rock's value of 1. For whole rock mass area is used the D-value of 0. Hoek-Brown parameter s determines cohesive properties of the rock mass and parameter an overall quality of the rock. These parameters can be calculated with equations (5) and (6).

$$s = e^{(GSI-100)/(9-3D)} \tag{5}$$

where GSI is the Geological strength index value
D is rock disturbance factor

$$a = 0{,}5 + \left(e^{-GSI/15} - e^{-20/3} \right) /6 \tag{6}$$

where GSI is the Geological strength index value

To model the strain-softening behavior of the rock with Hoek-Brown failure criterion, the residual values of the mb, s and a are needed. The residual values of Hoek-Brown parameters can be calculated by using the residual GSI factor and the disturbance factor for undisturbed intact rock. The residual value of GSI can be estimated using GSI reduction method by Cai et al. (2007). GSI is lowered based on changes in block volume and joint conditions with quantified the GSI-chart by Cai et al. (2004). Method is illustrated in Figure 4.

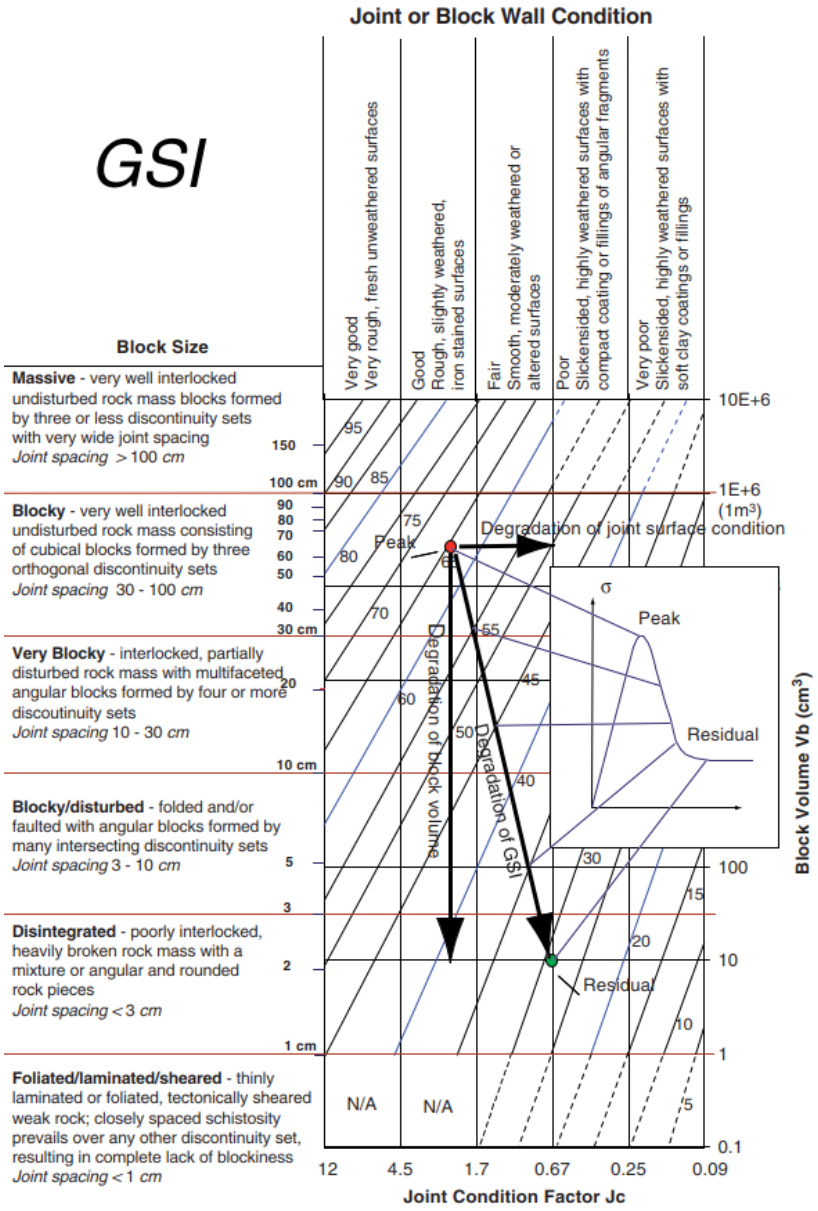

Figure 4 Determination of GSI_r by Cai et al. (2007)

$$m_r = m_i e^{(GSI_r - 100)/28} \tag{7}$$

where m_i is the intact rock quality parameter (MPa)
GSI_r is the Geological strength index residual value

$$s_r = e^{(GSI_r - 100)/9} \tag{8}$$

where GSI_r is the Geological strength index residual value

$$a_r = 0{,}5 + \left(e^{-GSI_r/15} - e^{-20/3} \right)/6 \tag{9}$$

where GSI_r is the Geological strength index residual value

Mohr-Coulomb failure criterion can also be written in relation between the major- and the minor stresses (Brady & Brown 2005). The friction angle and cohesion can be calculated from the Hoek-Brown parameters using equations (11) and (12) (Hoek et al. 2002).

$$\sigma_1 = \sigma_3 \frac{1+sin\varphi}{1-sin\varphi} + \frac{2c\ cos\varphi}{1-sin\varphi} \tag{10}$$

where σ_1 is the major principal stress magnitude
σ_3 is the minor principal stress magnitude
φ is the friction angle
c is the cohesion

$$\varphi' = sin^{-1}\left[\frac{6am_b(s+m_b\sigma'_{3n})^{a-1}}{2(1+a)(2+a)+6am_b(s+m_b\sigma'_{3n})^{a-1}}\right] \tag{11}$$

where a is rock mass quality parameter
m_b is reduced from constant m_i, rock mass quality parameter
s is rock mass quality parameter
$\sigma'_{3n} = \frac{\sigma'_{3max}}{\sigma_{ci}}$
σ'_{3max} is the maximum value of σ'_3 for equivalent Hoek-Brown and Mohr-Coulomb

$$c' = \frac{\sigma_{ci}\left[s(1+2a)+m_b\sigma'_{3n}(1-a)\right](s+m_b\sigma'_{3n})^{a-1}}{(1+a)(2+a)\sqrt{1+\left(6am_b(s+m_b\sigma'_{3n})^{a-1}\right)/((1+a)(2+a))}} \tag{12}$$

where σ_{ci} is the uniaxial compressive strength for intact rock (MPa)
s is rock mass quality parameter
a is rock mass quality parameter
m_b is reduced from constant m_i, rock mass quality parameter
$\sigma'_{3n} = \frac{\sigma'_{3max}}{\sigma_{ci}}$

3 Kemi mine

Kemi mine started as an open pit mine and after that mining transited to underground. Underground mine was constructed in four years, between the years 1999 and 2003. Underground mining was started two years before the open pit mining was finished in 2003.

The infrastructure for underground mining has been built to the footwall side, which is mainly hard granite. Underground mining started from level 550 and continued upwards towards bottom of the crown pillar on level 275 (Rikberg 2019). Currently Outokumpu is investing for expanding the underground mine to the level 1000, where new main level and drift is being built. Cross-section of mine is presented in Figure 5.

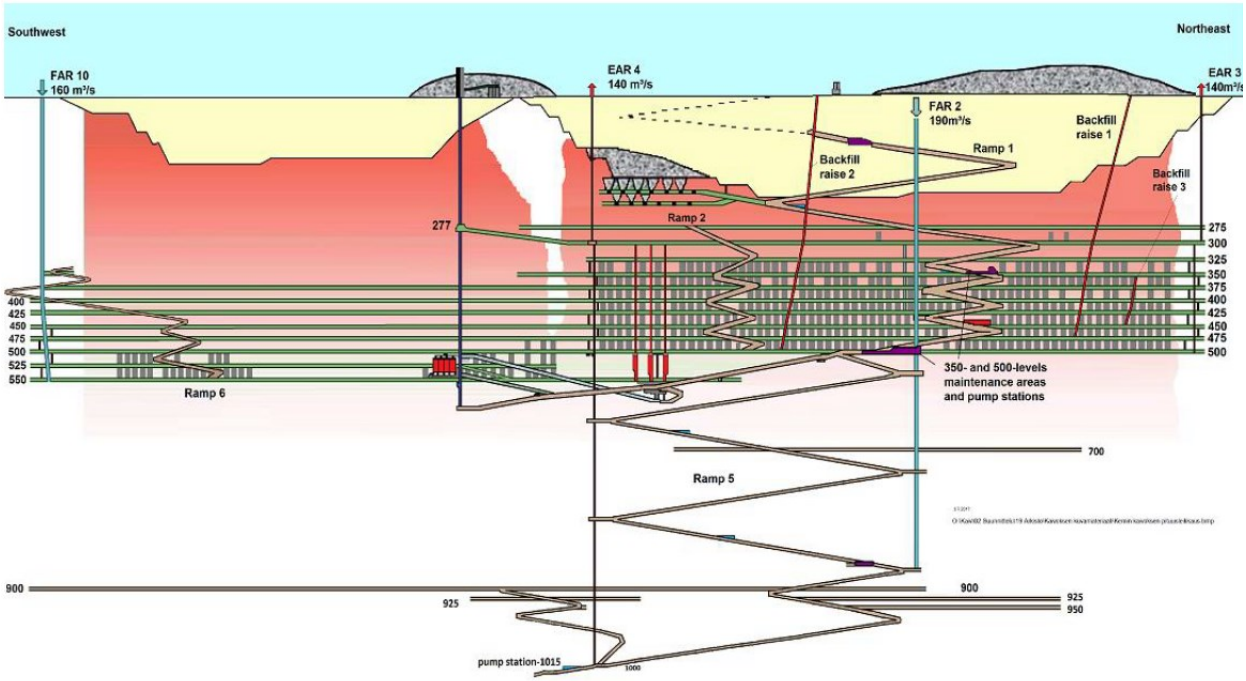

Figure 5 Simplified longitunal cross-section by Rikberg (2019)

Mining method for underground mining has been from the beginning to the present-day underground benching with back fill. Törmänen (2019) descripted in his master's thesis Kemi mine's used stope high to be 25 meters, -width varying from 12 to 18 meters and separation based on the used backfill. Stopes filled with mixture of waste rock and slurry are categorized as primary stopes and stopes filled with waste rock as secondary stopes. According Törmänen (2019) mining staff changes stope width with waste rock and pillars for stabilization of the mining area. Typical stope design is illustrated in the Figure 6.

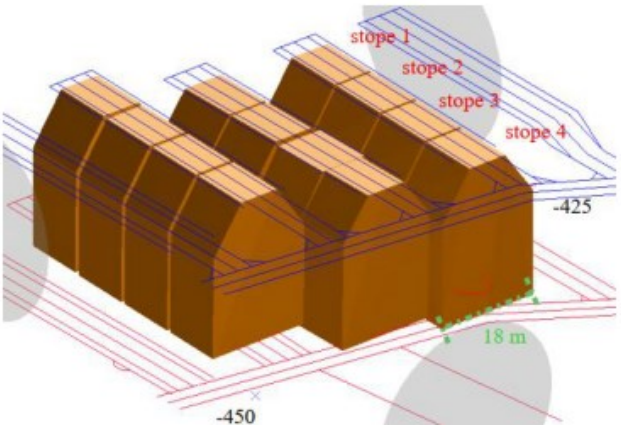

Figure 6 Ordinary stope design without pillars in SO orebody by Törmänen (2019)

The ore is crushed is concentrated in the plant as lumpy ore and fine concentrate products. Lumpy ores with sizes 10 – 120 mm are separated from the crushed ore using sink and float separation method. The sink and float method is based on differences in specifics gravities. The fine concentrate is separated from the crushed ore by using rod mills and spiral concentrators. Spiral concentrators separate the material by specific gravities. The tailings from the concertation are pumped to the spoil reservoir. In the reservoir the solid material is separated from the water and the water is pumped back to the concentration process (Salmi 2018).

As all used concentration methods are based on the gravitational separation, there is no usage of chemicals during the concentration of the ore. According to Salmi (2018) the annual productions are approximately for upgraded lumpy ore 400 000 tons and for fine concentrate 850 000 tons. The mine's effects to the surrounding environment are small due the chemical free concertation process, closed process water system and insolubility of the chrome ore's oxides. (Salmi 2018).

3.1 The geological environment- and stress state in Kemi mine

Kemi mines chromite deposit is part of Kemi layered intrusion. According to Huhtelin (2015) in the central part of the intrusion the main chromite layers length is around 1,9 km and average thickness is 40 m, decreasing outward from the center. The intrusion is estimated to be 3-4 km deep according to the geophysical seismic reflection surveys.

The Kemi layered intrusion has a lenticular shape, that is around 0,2-2 km wide and 15 km long according to Huhtelin (2015). Tectonic movements have tilted the intrusion to dip about 70 degrees to the northwest. The intrusion was metamorphosed during the Svecokarelidec orogeny. The surface view of the Kemi intrusion is represented in Figure 7.

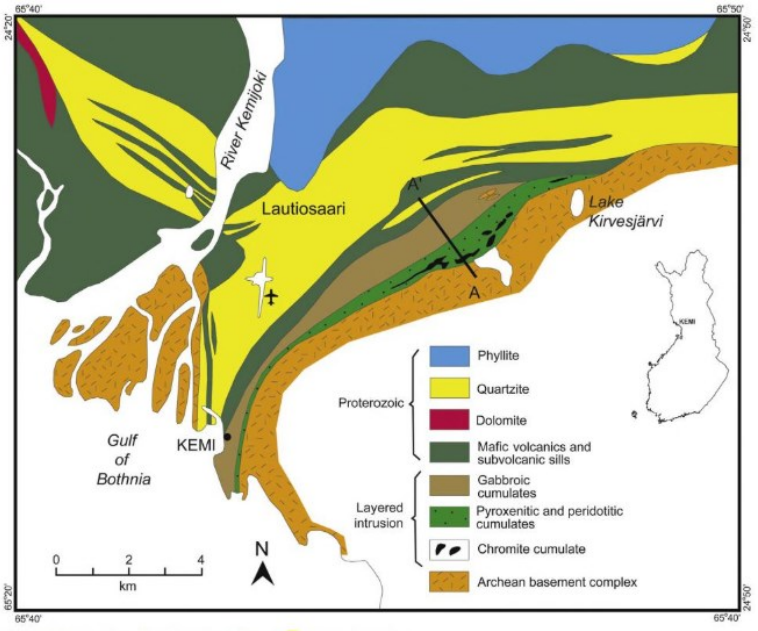

Figure 7 The Kemi intrusion by Huhtelin (2015) after Alapieti et al. (1989)

The chromite layer is mainly between metaperiodate layer on the hanging wall side and basalt contact series on the footwall side. The basalt series consist of mylonitic talc-chlorite-carbonate schist, talc-carbonate rock, metapyroxenite and irregular concentrates of gabbro. The basement granitoid is in contact with the talc-carbonate rock.

The ore body has been fragmented into a group of smaller ore bodies. The main orebodies illustrated in are: in northern part Pohjois-Viia (PV), in the middle Elijärvi (EL), in the western part both Surmaoja (SO) and Nuottijärvi (NJ). Smaller ore bodies are Mätäsoja (MO) to southwest-, both Länsi-Viia- (LV) and Itä-Viia- (IV) between EL and PV. The last smaller ore body is Viianmaa/Perukka (VP) to northeast from the main ore bodies. (Huhtelin, 2015).

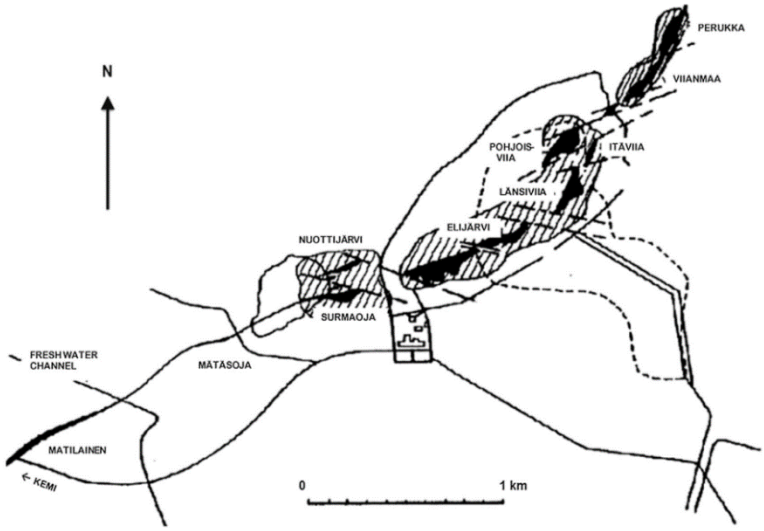

Figure 8 Main mining areas, lined areas are open pits by Huhtelin, T. (2015) after Alapieti et al. (1989)

Outokumpu Oy has data from stress measurements within the mine. These measurements have been taken from different levels within mine and used to determinate the stress state in the Kemi mine's bedrock. The measurements were carried out using overcoring and hydraulic fracturing. Due to uncertainties within conducted stress measurements caused by challenging rock conditions, used interpretation of maximum horizontal stress differs noticeably from linear curve fitting. The measurement results and interpretation points are shown in Figure 9.

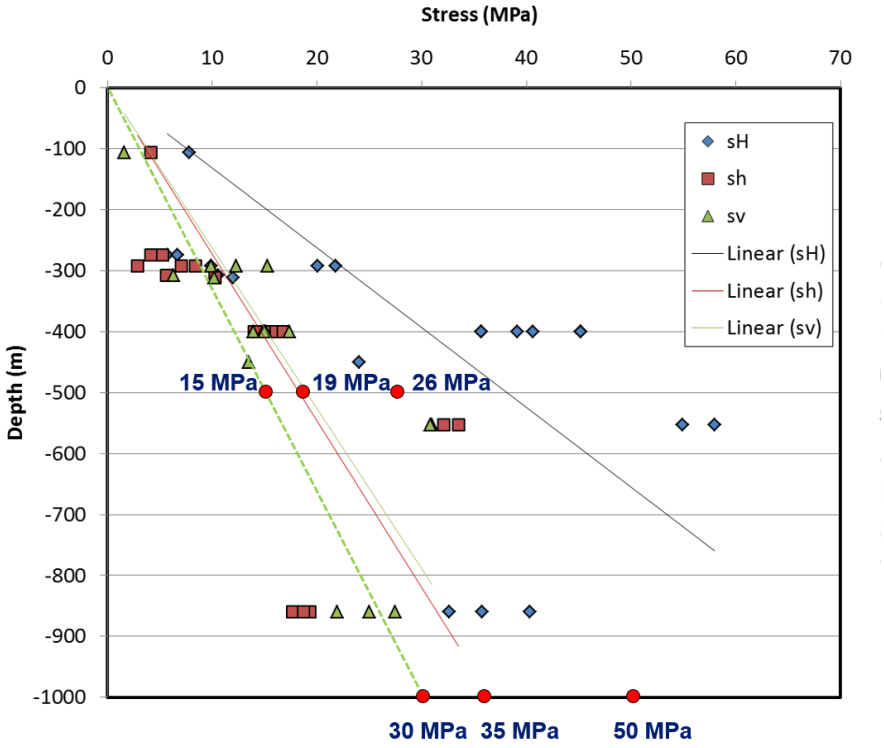

Figure 9 Plot of stress measurement results, interpretation points (red) used to determinate stress gradients

Direction of the maximum principal stress differs between 58 and 74 degrees in levels 400 and 860 according to the measurements. AFRY Oy has used interpret value for maximum principal stress of 66 degrees from north and intermedium principal stress 156 degrees from north. These stress directions were used in this thesis in setting the initial stress state within the model.

This means that complex stress state that exists within the mine is initially simplified. Stress state changes, when elastic equilibrium is calculated. This method has been used with success in rock mechanical simulations for the Kemi mine.

Initial stress state for simulations has been implemented via using stress gradients. Stress gradients with base point- and value are inserted to the FLAC 3D. Insertion format is axial stresses. Thus principal stress states are converted to axial stress states. Conversion is done by first converting stress states of interpretation points to axial stress values with equations (13) and (14). Minimum principal stress σ_3 is vertical stress and can be used without conversion. Next the stress gradients in Z-(vertical) direction between converted points are calculating using equation (15). Thus axial stresses are changing depending on the depth.

Stresses at base point of (0,0,0) are calculated in equation (16) with interpretation point and stress gradients in Z-direction.

$$\sigma_x = \sigma_{1ip} * COS(\alpha)\text{^}2 + \sigma_3 * SIN(\alpha)\text{^}2 \quad (13)$$

where σ_1 is the major principal stress at interpretation point
σ_3 is the minor principal stress at interpretation point
α is the angle from model's x-axis (from north)

$$\sigma_y = \sigma_{1ip} * COS(\beta)\text{^}2 + \sigma_{3ip} * SIN(\beta)\text{^}2 \quad (14)$$

where σ_1 is the major principal stress at interpretation point
σ_3 is the minor principal stress at interpretation point
β is the angle from model's y-axis (from north)

$$\sigma_{i\Delta Z} = \frac{\sigma_{iP1} - \sigma_{iP2}}{H_{P1} - H_{P2}} \quad (15)$$

where $\sigma_{i\Delta Z}$ is axial stress gradient
σ_{iP1} is axial stress i at interpretation point 1
σ_{iP2} is axial stress i at interpretation point 2
H_{P1} is the depth of interpretation point 1
H_{P2} is the depth of interpretation point 2

$$\sigma_{iP0} = \sigma_{iP} + \sigma_{i\Delta Z} * H_P \quad (16)$$

where σ_{iP0} is axial stress at base point (0,0,0)
σ_{iP} is axial stress i at interpretation point
$\sigma_{i\Delta Z}$ is axial stress gradient
H_P is the depth of interpretation point

4 Building the simulation model

In this chapter is explained the way simulation model has been constructed. This includes used the stress analyze method, geometry of the model, parameters and the chosen approach to simulate the effects of mining with each mining method.

4.1 Finite difference method as a stress analyze method

The finite difference method calculates the unknown parameters from the known quantities using set of differential equations. The solution is calculated in step by step fashion, where in theory the solution is closer to the equilibrium after each step. Thus reaching the

equilibrium solution requires no matrices. This reduces the required memory needed for calculations especially, when meshes containing immense amount of elements are used (Brady & Brown 2005).

The downside of using differential equations to conduct stress analyses is the computational time needed to reach the step that can be considered equilibrium solution or an acceptable unbalance within the model (Brady & Brown 2005).

The finite difference model is constructed by forming the wanted body from quadrilateral elements. Medium's constitutive equations and laws of motion dictates the differential equations within each element. Elements are connected to each other's via grid points. Solving of the differential equations is started from the unbalanced force from different elements at grid points. Typically elements between gridpoints are called "zones". The Finite difference grid and -point to zones interrelationship is represented in the Figure 10 below. (Brady & Brown 2005).

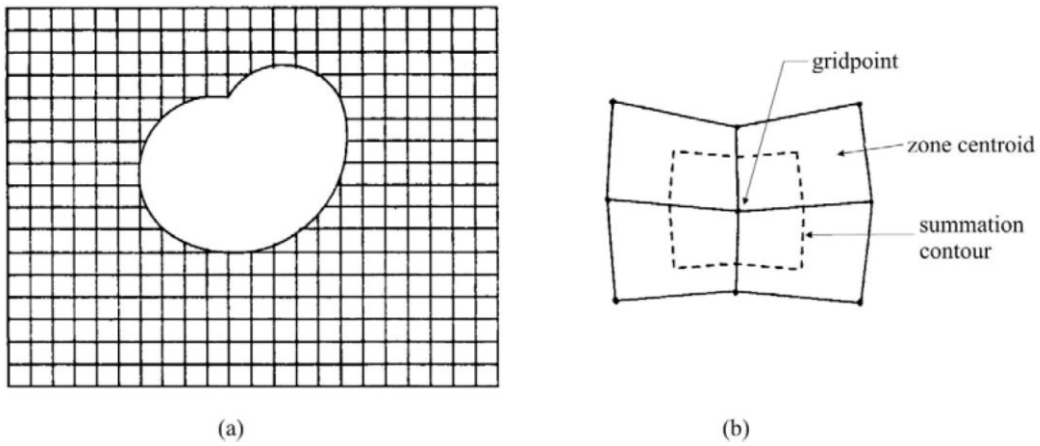

Figure 10 Illustration of: a) example of finite difference grid, b) affecting areas to gridpoint by Brady & Brown (2005)

Calculation procedure starts with solving the resultant of all forces at the gridpoint. This is called out-of-balance force at gridpoints. Next is acceleration, velocities and displacements are calculated from the out-of-balance forces. Finally strains are solved from accelerations with constitutive equations. (Brady & Brown 2005).

Used software in this theses, the FLAC 3D calculation sequence is: first strain rates are derived from gridpoint velocities, then stresses are calculated from new strain rates using constitutive equations. And finally new nodal velocities and displacements are solved from the equations of motion with stresses and forces. This calculation procedure repeated at every timestep. (FLAC 3D, 2017).

4.2 Geometry of the simulation model

The model has five major geometries and three minor geometries. These geometries are either constructed within the constructed mesh or imported to the model. The major geometries within the model are:

- Granite (GR) on foot wall side
- Talc-carbonite (TLKKRB) from granite on foot wall side to metaperiodate on hanging wall side,
- Orebody within talc carbonite,
- Metaperiodate (MPRD) on hanging wall side,
- Current open pits

Minor geometries are added to represent geology and rock mass structure more accurately near ground surface and between levels -500 and 0. These minor geometries are:

- Metapyroxenite (MPYR), rock that has weak uniaxial compression strength.
- Weakness-zone, areas that has been identified with geological interpretations as weakness-zones.
- Mining off-limit areas, areas within mine that haven't been excavated during underground excavations such as crow pillars and supporting pillars within ore body.

The mesh has been constructed with Rhinoceros-software and imported to the FLAC3D. Figures 11-18 are from the FLAC 3D model. The mesh's width is 6000 m, length 3500 m and height 1600 m. Zone edge length vary in the model from 5 m to 130 m and the total amount of zones is a little bit over 4,5 million. Ore body contains the smallest zone edge lengths and the rest of the mesh is constructed based on the ore body's mesh.

After the mesh of the model has been imported to the FLAC3D, the ore body has been separated in smaller ore bodies based on the location of the ore body. This separation enables more accurate representation of excavation plans within simulations. After the separation, ore bodies are divided in different excavation levels with 25 m high, that is same as stope height. Stope geometries are used for the levels that Outokumpu has provided for UGB or SLC mining. Other mining levels are excavated completely in the model. Outokumpu Oy has provided stope geometries of UGB mining for levels 550-600 and 1000-1200. SLC stope

geometries were provided by Outokumpu Oy for levels 575-725 and 1000-1200. After the ore body have been divided by ore body location and mining levels, geometries of the different rock regions are imported to the model.

Simulation model's geometry is illustrated in the Figures 11-18. The ore body is shown as a red area within the model. In the Figure 11 on left side is picture of the model from the top and on the right side is cross-section from middle of Elijärvi open pit. Open pits are within green areas in the Figure 11. In the middle is the Elijärvi (EL), west- and north Viia (PV) open pit. On the south-west side of it is the Surmaoja (SO) open pit and in the north-east side is the Viianmaa-Perukka(VP) open pit. Major geometries of the model are represented in the Figures 11-15 and minor geometries in the Figures 15-18.

Geology surrounding the ore body is constructed by importing geometries of rock regions other than granite and talc-carbonite to the model. Granite region covers almost half of the model and it is on the southern side of the model. Talc-carbonite region is in the middle of the model with ore bodies, weakness zones and meta pyroxenite. Talc-carbonite region will be formed from the remaining area after geometry of metaperiodate has been imported to the model. Remaining smaller geometries are then imported and carved from the major geometries.

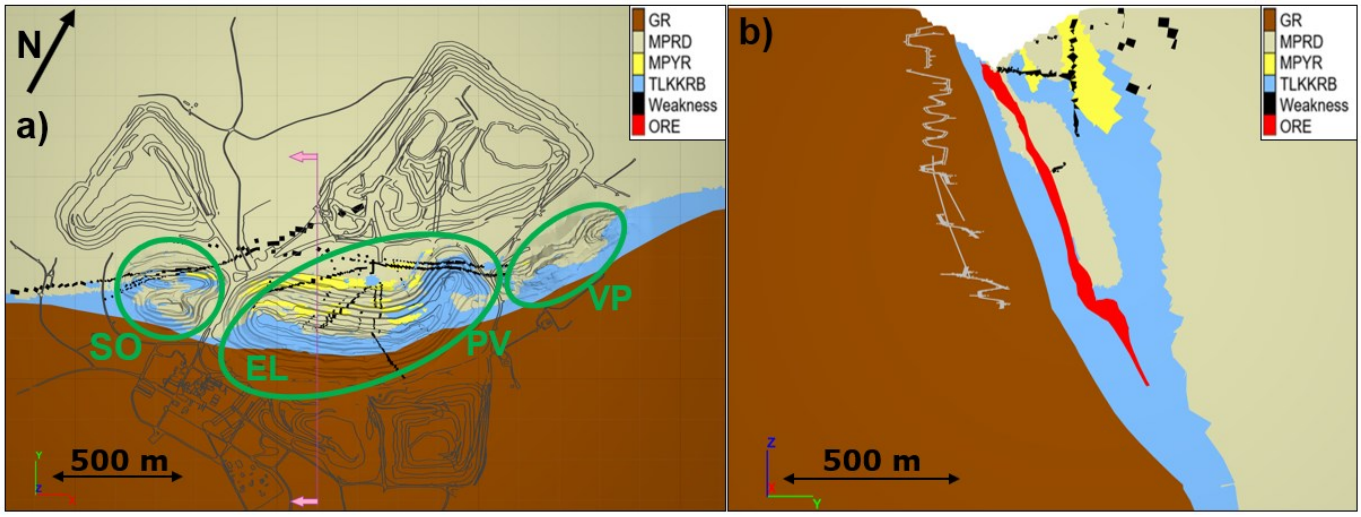

Figure 11 Rock types and weakness zone on ground surface and from cross-section

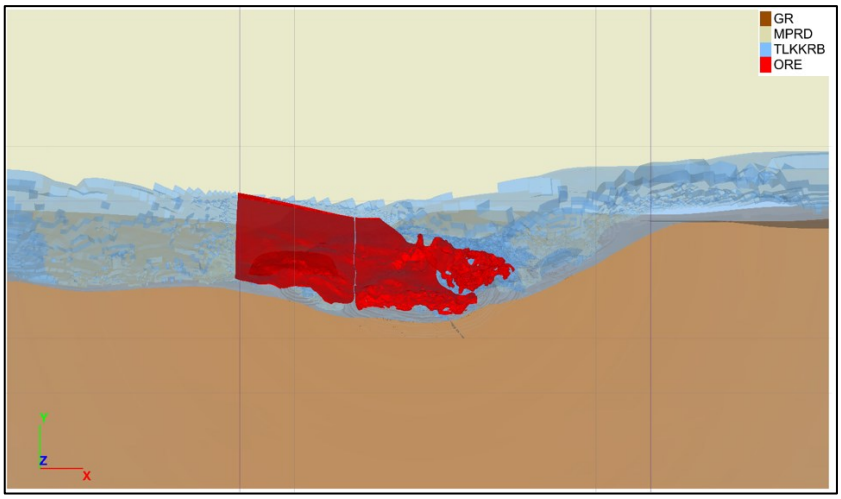

Figure 12 Major geometries from the top

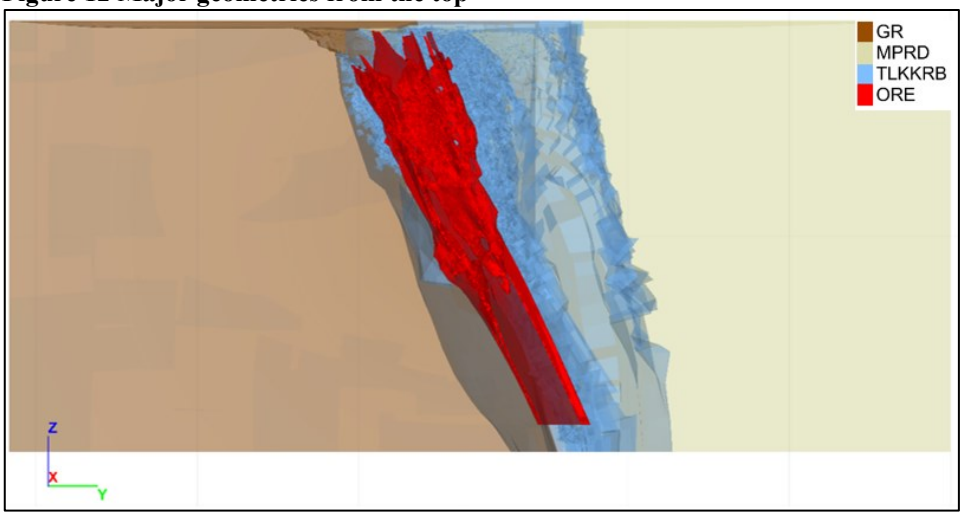

Figure 13 Major geometries from the side

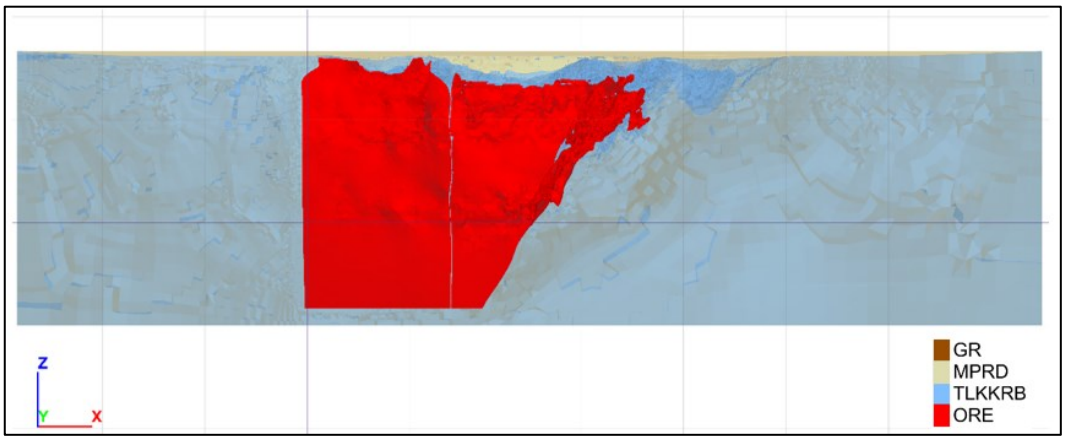

Figure 14 Major geometries from the front

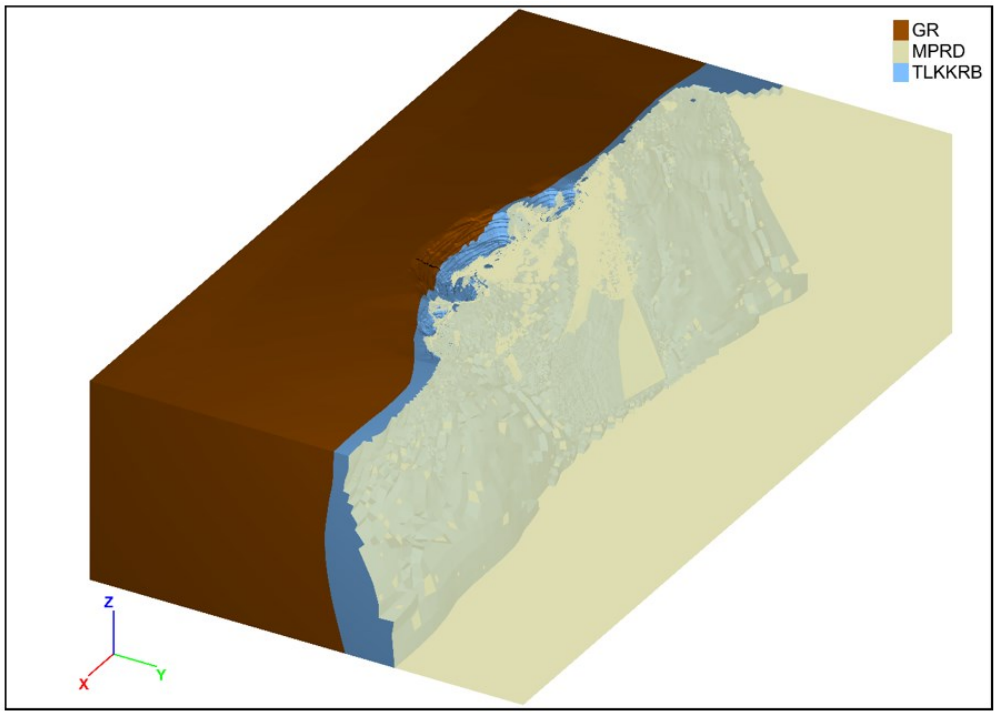

Figure 15 Isometric plot of the major rock types within the model

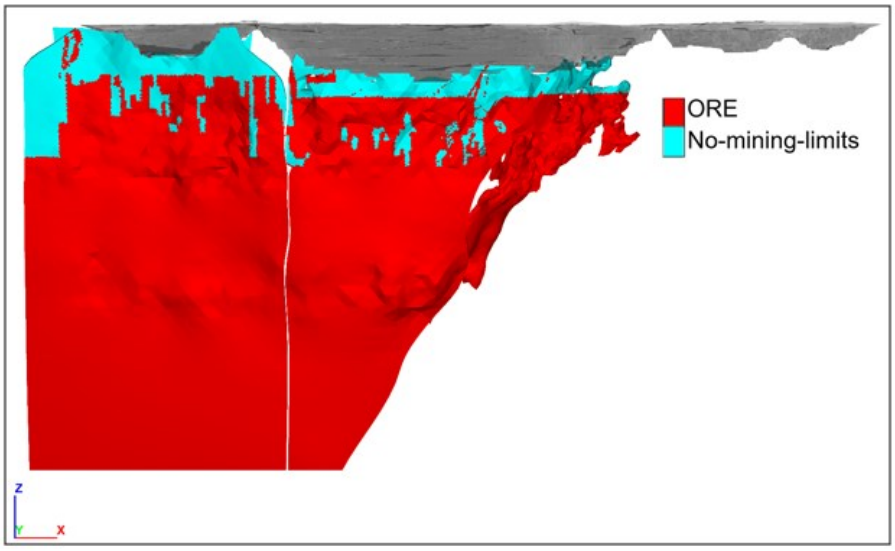

Figure 16 No-mining-limits-geometry on orebodies, mainly crow pillar and supporting pillars within ore body

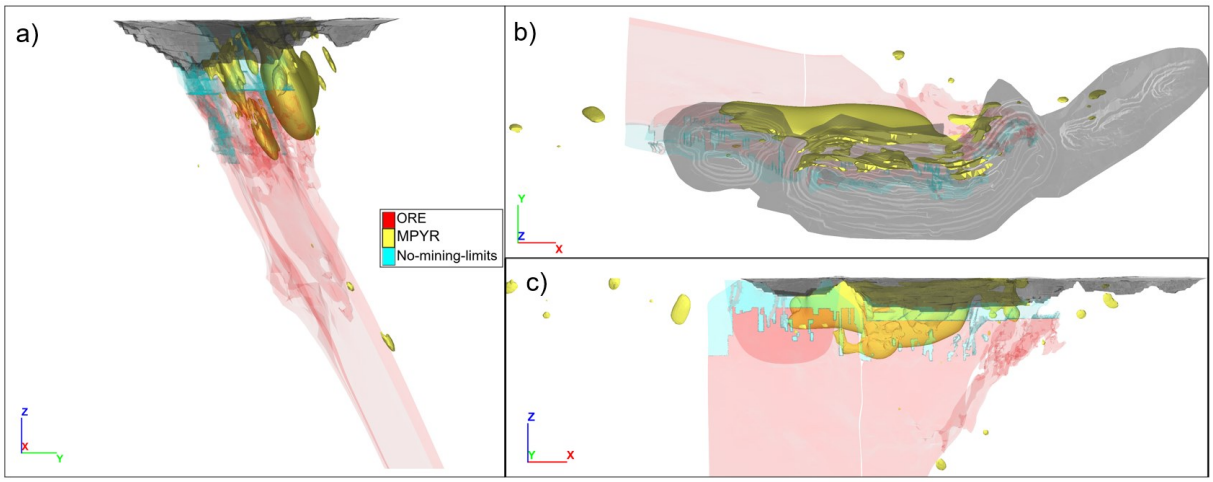

Figure 17 Geometry of metapyroxenite from a) side-, b) top- and c) front of the model

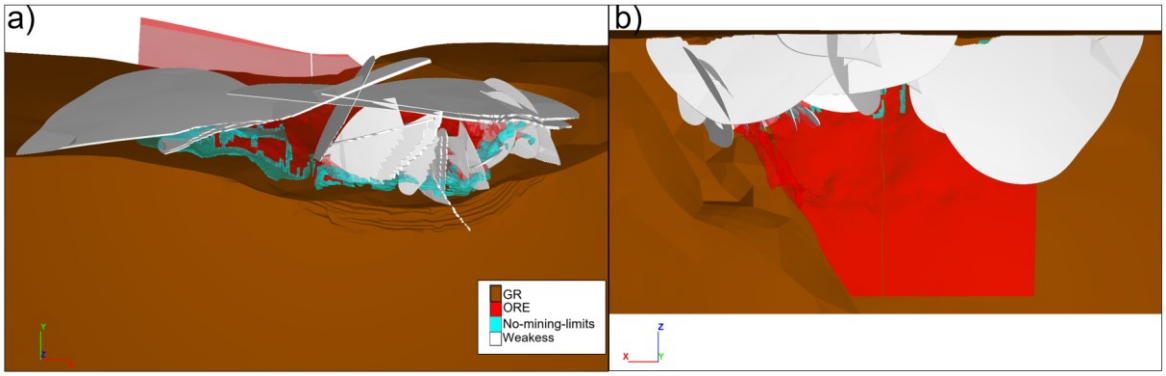

Figure 18 Geometry of weakness zones from a) top- and b) front of the model

4.3 Determination of the parameters/ simulation parameters

Determination of the used parameters for simulations is one the most important part of the thesis as the chosen parameters have immense influence on the results of the simulation.

The bed rock's mechanical properties vary within the mine's vicinity. The granite on the footwall side can be considerate as good quality hard rock mass whereas the rock mas within the basalt zone is poor quality medium hard rock with gabbro concentrates being exception. The Hanging wall side metaperiodate is hard rock, however the weakness zones and faults locally reduce its mechanical properties drastically. Outokumpu Oy has data from laboratory tests and - drill core samples. The important mechanical properties of the rock mass for the simulations are:

- Uniaxial compression strength (UCS) for intact rock, σ_{ci} (MPa). The σ_{ci} is evaluated from uniaxial compression tests. It refers to intact rock's ability to bear compression stress without breaking.
- Geological Strength Index, GSI (-). The GSI value is taken from drill core analyses. Meaning of GSI values has been discussed in chapter 2.1.

- Intact rock strength parameter, m_i (-). The mi value for the rock is taken from the table by Brady & Brown (2005), after Hoek (2003). Same as GSI, the m_i is explaned more thoroughly in chapter 2.1.
- Young's modulus for intact rock, E_i (GPa). Young's modulus is interpreted from the uniaxial compression tests. Young's modulus describes stiffness of the rock mass and thus links to the magnitude of strains and- displacements within rock mass. The E_i is used to calculate Young's modulus for the whole rock mass.
- Poisson's ratio, v (-), The Poisson's ratio is also is interpreted from the uniaxial compression tests and it connects different axial strains to each other under stresses.
- Unit weight (kg/m^3). The value for rock's unit weight is taken from drill core analyses.
- Dilation angle (°). The dilation angle of the rock is evaluated using method by Hoek (2001). Dilation expresses rock masses volumetric expansion under shear strain.
- Peak tensile strength (MPa) of the rock mass. The peak tensile strength is calculated using Hoek-Brown failure criterion.
- Bulk modulus, K (GPa). The K is calculated from E and v.
- Shear modulus, G (GPa). The G is calculated from E and v.

The σ_{ci}, GSI, E_i, v are used to calculate failure criterion parameters in chapter 2.2.
The used values of these mechanical properties of the rock masses are discussed in chapter 4.4.

Rock mass dilation has been determined in this thesis for each rock type according the category created by Hoek (2001). In this category the dilation is calculated differently based on overall quality of the rock mass by emphasizing good quality rock has higher dilation than average- or poor quality rock. The category is shown in the Table 1 below.

Table 1 Rock mass dilation by Hoek (2001)

Rock mass quality	Dilation
Very good	Phi/4
Average	Phi/8
Poor	0

Rock masses tensile strength can be approximated by inputting σ_1=σ_3=σ_{tm} in Equation (3). This will results in: (Brady & Brown 2005)

$$\sigma_{tm} = -s\sigma_{ci}/m_b \quad (17)$$

where s is rock mass quality parameter
σ_{ci} is the uniaxial compressive strength for intact rock (MPa)
m_b is reduced from constant m_i, rock mass quality parameter

Rock mass properties used in simulations are calculated from intact rock properties and applied to model. Youngs modulus of the rock mass can be calculate using equation (18) by Hoek & Diederichs (2005).

$$E_{rm} = E_i\{0{,}02 + ((1 - D/2)/(1 + e^{(60+15D-GSI)/11}))\} \quad (18)$$

where E_i is the deformation modulus for intact rock (MPa)
D is rock disturbance factor
GSI is the Geological strength index value

$$G = \frac{E_{rm}}{2(1+v)} \quad (19)$$

where E_{rm} is the deformation modulus for rock mass (MPa)
v is the Poisson's ratio

$$K = \frac{2G(1+v)}{3(1-2v)} \quad (20)$$

where G is the shear modulus for the rock mass(MPa)
v is the Poisson's ratio

In order to simulate strain-softening behavior of the rock mass the required plastic strain of rock to reach it's residual strength is needed. This cumulated plastic strain increment is typically referred as a critical plastic strain. Critical plastic strain depends on the rock mass structure and studied element size in the model (Sainsbury 2012). It can be estimated with equation (21) (Sjöberg et al. 2017).

$$\in_{crit}^{ps} = 12.5 - \frac{0.125GSI}{100\Delta z} \quad (21)$$

where GSI is the Geological strength index value
Δz is the length of the zone's edge

Rock strength and structure parameters for metamorphic peridotite (metaperiodate) are determined by tuning a calibration simulation model's displacements and plastic strains to correspond measured in-situ displacements and cracks on the surface. The post-peak behavior of the hanging wall rock is controlled by reducing values of Hoek-Brown parameters rock strength parameter mb and rock intact parameter s. Values of mb, s and a change linearly from peak to the residual values. The determination of peak and residual values for m, s and a are discussed in chapter 2.2.

Table 2 Simulation parameters for Mohr-Coulomb materials

Mohr-Coulomb, no strain softening	GR	Fill
Unit weight (kg/m3)	2650	1850
Tension (Mpa)	0.91	0.05
friction angle	54.05	35
cohesion (Mpa)	7.63	0.10
dilation (°)	6.80	0
bulk modulus K (Gpa)	41.2	9.5E-05
shear modulus G (Gpa)	23.6	6.4E-05

Table 3 Simulation parameters for Hoek-brown with strain-softening materials, Metaperiodate(MPRD), Talc-carbonite (TLKKRB), Orebody (ORE), Metapyroxenite (MPYR)

Hoek.-Brown, strain softening	MPRD	TLKKRB	ORE	MPYR	Weakness
Uci (Mpa)	120	50	72	35	30
GSI (-)	55	55	60	50	44
GSIr (-)	20.0	20.0	21.8	18.2	16.0
mi (-)	6.3	10	10	5	10
Ei (MPa)	60000	39000	56000	30000	30000
Poisson v (-)	0.27	0.30	0.33	0.20	0.30
Unit weight (kg/m3)	2900	3000	3500	2900	3000
dilation (°)	4.99	4.62	4.99	0	0
bulk modulus K (Gpa)	17.75	13.3	28.5	5.12	5.23
shear modulus G (Gpa)	9.64	6.12	10.95	3.84	2.42

Table 4 Strain-softening parameters for metaperiodate

MPRD	Strain softening table			Critical plastic strain	
strain	0	0.00100	0.0015	0.0020	0.3
a	0.512	0.513	0.519	0.535	0.544
mb	0.697	0.653	0.475	0.0252	0.362
s	1.20E-03	1.12E-03	8.07E-04	2.79E-06	0.0001379
Tension	6.40E+05	6.40E+04	3.84E+04	1.28E+04	0.00E+00

Table 5 Strain-softening parameters for Talccarbonite

TLKKRB	Strain softening table			Critical plastic strain
strain	0	0.001	0.005	0.0113
a	0.504	0.506	0.515	0.529
mb	2.00	1.83	1.14	0.0518
s	6.74E-03	6.14E-03	3.75E-03	4.64E-06
Tension	1.70E+05	1.70E+03	1.70E+02	0

Table 6 Strain-softening parameters for ore body

Ore	Strain softening table			Critical plastic strain
strain	0	0.001	0.005	0.0100
a	0.503	0.505	0.515	0.528
mb	2.397	2.162	1.225	0.0538
s	1.17E-02	1.06E-02	5.87E-03	5.07E-06
tension	3.50E+05	3.50E+03	3.50E+02	0

Table 7 Strain-softening parameters for metaphyrite

MPYR	Strain softening table			Critical plastic strain
strain	0	0.001	0.005	0.0125
a	0.506	0.508	0.515	0.530
mb	0.838	0.773	0.513	0.0246
s	3.87E-03	3.56E-03	2.32E-03	4.11E-06
tension	1.60E+05	1.60E+03	1.60E+02	0

Table 8 Strain-softening parameters for weakness zones

Weakness	Strain softening table			Critical plastic strain
Strain	0	0.001	0.005	0.014
a	0.509	0.510	0.517	0.533
mb	1.353	1.260	0.886	0.045
s	1.98E-03	1.84E-03	1.28E-03	3.37E-06
tension	1.60E+05	1.60E+03	1.60E+02	0.00E+00

4.4 Approaches to simulate effects of the mining

The simulation scenarios are constructed using short calculation phases and examination phases. During examination phase the model is cycled to equilibrium. Short calculation phases are used to simulate changes in model in time saving fashion. The amount of examination phases within scenario is two. In the Appendixes 2,3,4 and 5 are the mining sequences for all the different mining scenarios studied in this thesis.

One simplification done in model is that mining levels haven't been divided between hanging- and foot wall. This means that mining levels are excavated wholly, without leaving any supporting pillars between stopes. Thus in simulations the typical advance of the empty space within stopes and mining levels can't be simulated.
In all simulations excavated mining levels are only within the ore body.

The reason to examine only two points during the simulation of the scenario is to reduce the total of time that simulations are taking. This means that study of more accurate propagation of displacements and evolving of the stresses within rock mass is traded for much shorter total simulation time. This is reasonable tradeoff as otherwise the simulations would take unacceptable amount of time and with two comparison points, the overall behavior of the simulation scenario can be captured.

4.4.1 UGB with fill

During underground benching with fill, first the ore is mined and later filled with backfill. As the backfilling isn't instant, the level will be empty for a short amount of time. This cycle of excavation and back filling is continued starting from bottom of the excavation area and advancing towards the ground surface until all desired area has been excavated.

To simulate this mining method's effect to the rock mass, firstly the ore from the current mining level is excavated. In the simulation the excavation is done by changing the excavated zones into an empty space by removing all material properties and failure criterion. This operation is done by assigning excavated zones constitutive model as "null"

After the level has been excavated, it will be empty for a short time period before and during back filling (Figure 19 b) phase 0). This is done in simulations by letting the level being empty for one calculation phase and then filled with backfill. The back filling is done in simulations by assigning zones within back filling area to have failure criterion and needed material properties of backfill. After level has been filled, following level in mining sequence is excavated. This calculation cycle is repeated until an examination phase is reached (Figure 19 b) phase 1-3). This logic sequence is illustrated in Figure 19.

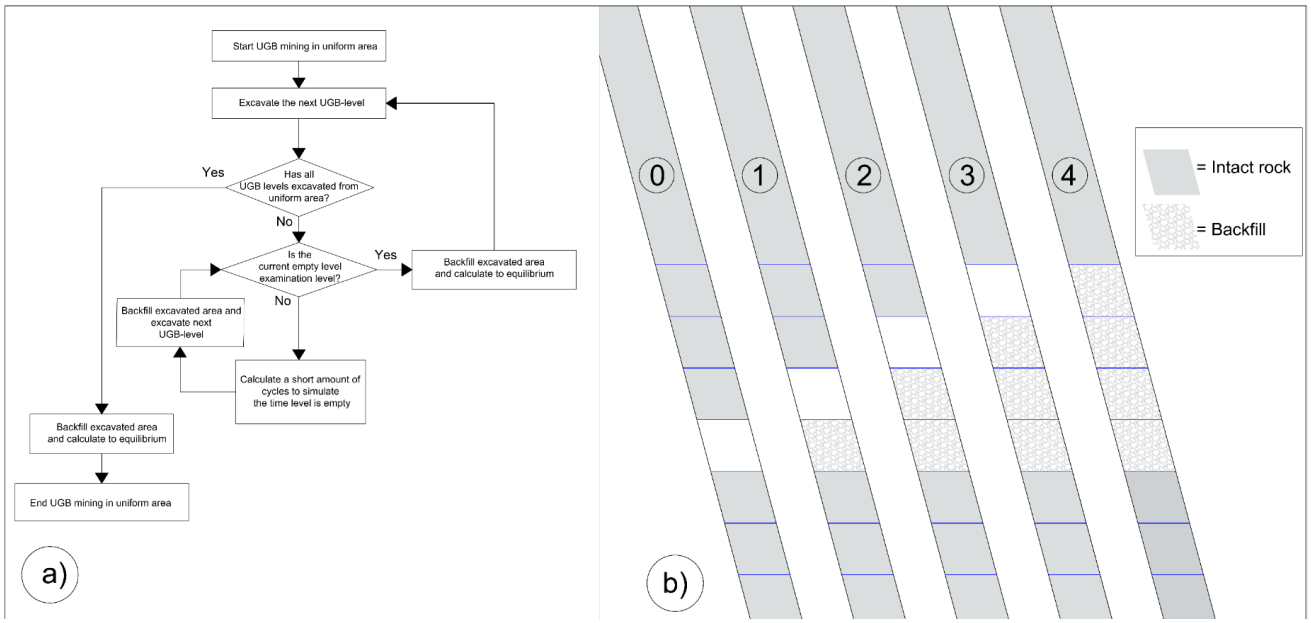

Figure 19 a) Flow chart of UGB simulation logic, b) Illustration of logic sequence

4.4.2 SLC method

SLC mining method is used in hard rock mass, where the caving is transitional and isn't self-sustained nor -induced. The SLC is initiated for each mining stope by blasting. In the best scenario, hauled rock contains only slight amount of the caved hanging wall waste rock. Typically in SLC-mining the stopes are excavated from the back of stopes to the foot wall drifts. Also commonly after stope has started to cave in to the stope, excavation in underneath stopes is started. That way the unsupported wall area is increased and caving from the roof is transferred to the wall side. Sublevel caving is presented in the Figure 20.

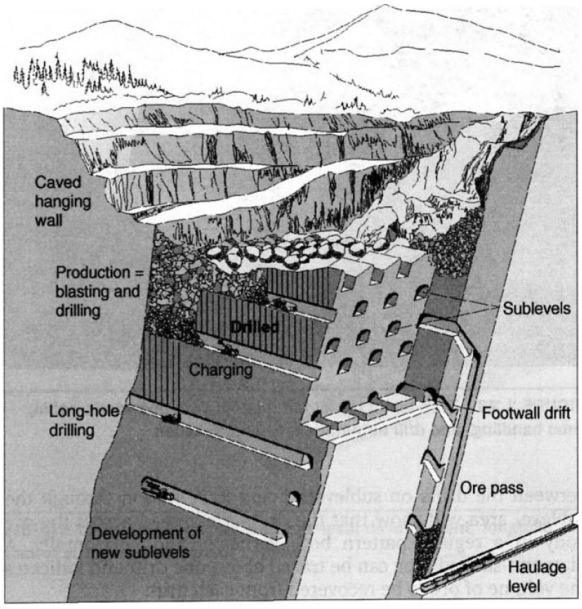

Figure 20 Sublevel caving layout by Hamir (2001)

In this thesis the focus is to examine the consequences of SLC mining for the mine's stability, not the rock flow within excavated- and caved areas. Excavation of the level is done in simulations in the same way as the empty cavern was created in the UGB with fill.

First assumption is that caved area from the walls and roof have similar total displacements than mobilized zone would typically have. As such areas with total displacements of one meters or greater are interpret to be fully loose rocks.

Second assumption is that loose rocks will fall down from the roof and the walls and distribute evenly to the bottom of empty cavern formed by excavated levels and caved area. As such caved rock forms support to excavated areas, always filled upwards from the lowest excavated mining level.

Third assumption transforms excavation induced caving area to fully bulked rocks. Sainsbury, B. (2012) discussed that rock masses typical value for bulking factor to be 43 %, that is used for calculate caved rock areas this thesis.

From these three assumptions can be calculated the area and thus the levels where the caved rocks provides support within the production area The area of caved rocks is calculated with equation (22) and upper level of caved rocks by equation (23).

$$A_{Caved\ rocks} = A_{Caving\ area} * (1 + B_{max}) \quad (22)$$

where $A_{Caving\ area}$ is the area of excavation induced caving (m^2)
B_{max} is the theoretical maximum bulking factor for rocks

$$N_{levels\ of\ rock\ support} = \frac{A_{Caved\ rocks}}{A_{Average\ mining\ level}} \quad (23)$$

where $A_{Caved\ rocks}$ is the area of excavation induced loose rocks (m^2)
$A_{Average\ mining\ level}$ is the area of average mining level (m^2)

These assumptions and equations were used to create SLC mining logic sequence. The logic sequence consist of one main calculation - and two side calculation cycles. The main cycle is used to study cave propagation and side cycles are used to record changes in model. The sequence is presented in the Figure 21.

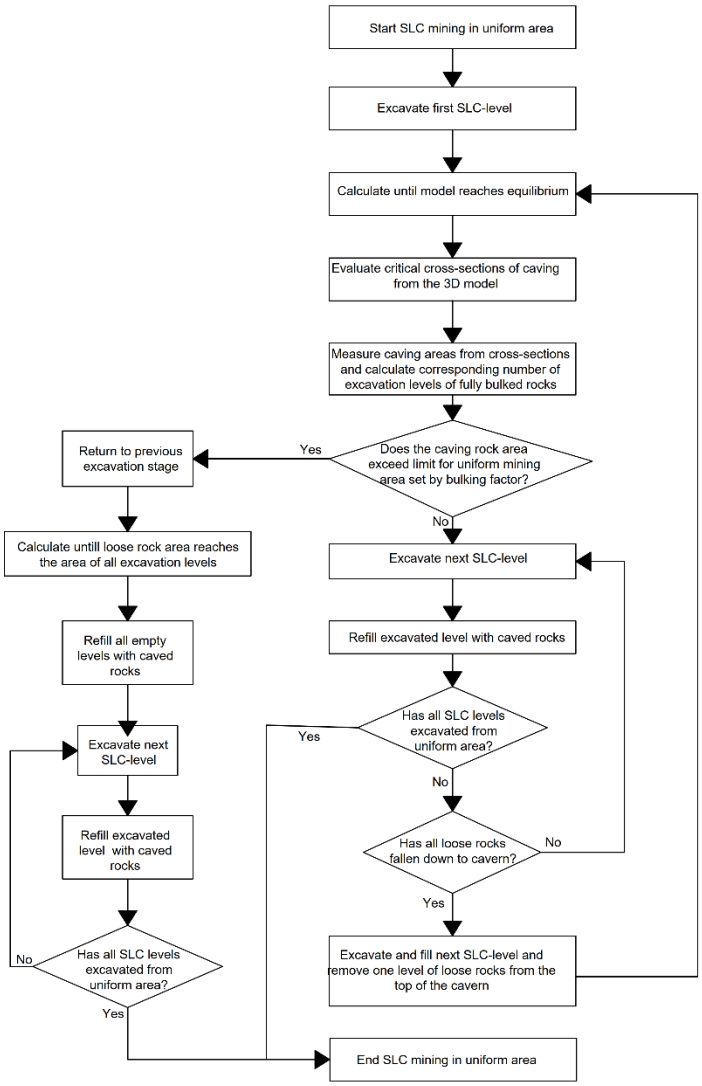

Figure 21 Flow chart of logic sequence created in this thesis to simulate effects of SLC-mining

The main cycle is illustrated in the Figure 22 and stages within it are:

- 0-1, Beginning of main cycle, first level has been excavated from the ore body. Newly excavated area causes the rock mass around it to cave into the empty cavern. Area of interpreted caving area represent the caving area if the excavated level would be constantly kept empty. However, in reality once the caving starts, fallen rocks will support the cave, thus slowing the caving process and eventually stop the caving completely. Caving area is interpreted from the results and then used to calculate equivalent excavation levels of caved rock. In short how many levels needs to be excavated to reach such state within the production area.

- 2-5, These stages represent repeating phases within the main cycle. Caving area caves into the cavern until the support from the loose rocks stabilize the caving. After new level is excavated the loose rocks fall down to the bottom of the cavern and caving will resume. This of caving and excavation is repeated until the amount of excavation levels of caved rock equals to newly excavated levels. Interpreted caving area isn't fully removed from the model, this is done in part to preserve model stability and -software limitations.
- 6, a new level has been excavated from the ore body and loose rocks tumble down to the bottom of the empty level, enlarging empty area in upper part of the cavern.
- 7-8, Enlarged empty area in the upper part causes caving to continue and creates similar state than phases 0-1.

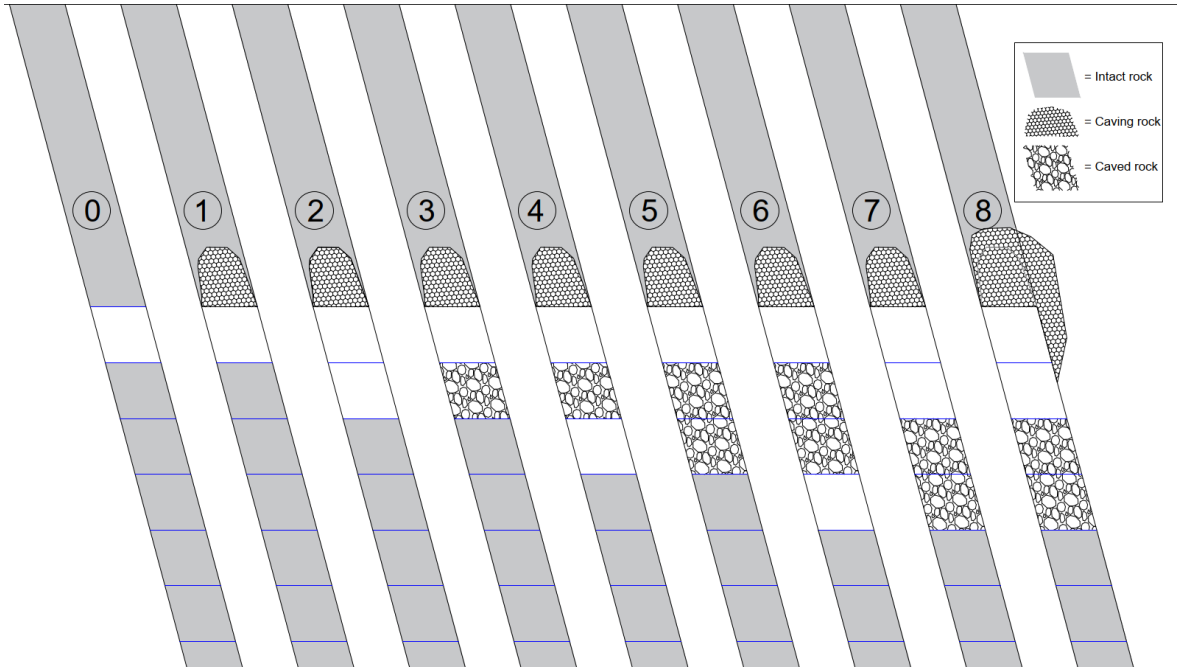

Figure 22 Illustration of logic sequence to simulate SLC mining

5 Simulations and -results

All scenarios start from the current state of the mine. Then used mining order and – method will depend on the studied scenario. All scenarios can be divided in two parts. In the first part includes the mining of the rest of current underground mine and the upper half of the new underground mine expansion called Deep Mine. This upper half of the Deep Mine expansion is called Deep I. After Deep I has been excavated, the lower half of the Deep mine called Deep II is excavated.

Deep I will be mined after or at the same time that SO levels -375 to -175 are mined with UGB, depending on the studied scenario. Level -1000 divides the Deep mine into upper and lower half. Deep I ranges in the EL- and PV area from level -550 to level -1000. In the SO area it contains less levels as the range is from -600 to -1000.

Deep II consist of levels -1000 to -1500 in all areas. It is noteworthy to point out that PV areas has no excavated area in the Deep II and that EL area convergences with depth so that at the bottom of Deep II the width of excavated area is only approximately one quarter of the width near surface. Different mining scenarios are illustrated in Figure 23 Illustration of different mining scenarios. S stand for "scenario" and I or II as a Deep mine I or II. Figure 23 and mining orders of them are represented in the appendix 2-5 and are in same order as in the list of scenarios bellow:

- Scenario 0: All mining areas are mined with UGB method.
- Scenario 1: All mining areas are mined with SLC method.
- Scenario 2: Deep I levels – 950 to -825 mined using UGB and levels – 550 to -825 using SLC. Deep II mined using SLC.
- Scenario 3: Deep I EL area mined using UGB. Every other area including whole Deep II mine mined using SLC.

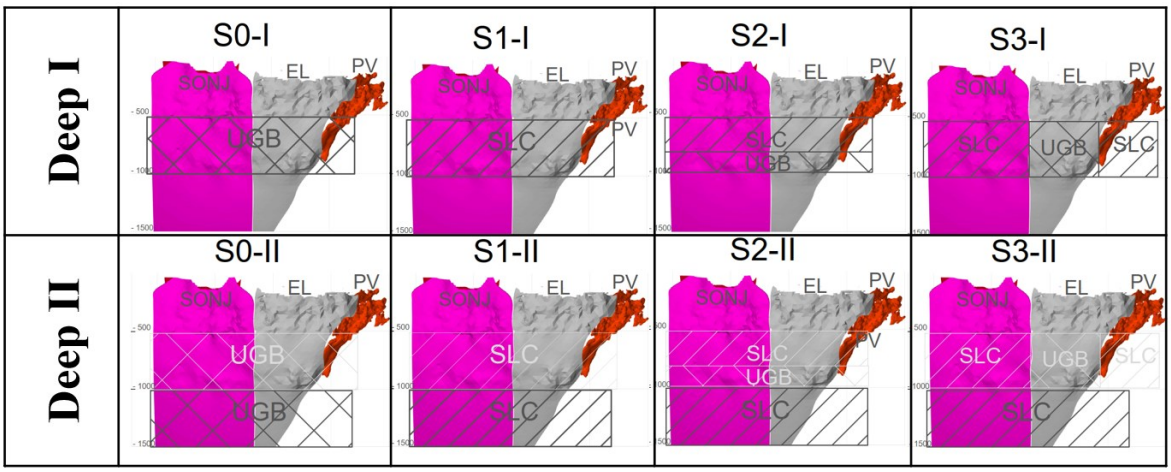

Figure 23 Illustration of different mining scenarios. S stand for "scenario" and I or II as a Deep mine I or II.

The current state of the mine consists of underground mining from levels -275 to -500 in EL- and PV areas. From SO area levels -375 to -550 have been excavated, also two horizontal pillars have been excavated. At the current state of the mine there are tensile failure cracks at the ground surface around the Elijärvi-Pohjois-Viia open pit and on the

hanging wall side. These cracks are represented as white lines and – dots in plastic strain plot of Figure 24. From the Figure 24 can be seen that the locations of existing cracks at the surface corresponds mostly with areas with plastic strain higher than $4e^{-4}$ (0,04%). Current total displacements at the ground surface are focused at the hangingwall side of the ELPV open pit and are around 20 cm in magnitude. This is illustrated in the Figure 25 below. Form it can be seen that vertical displacements are 5-10 cm in magnitude. By comparing displacements from the Figure 25 and the Figure 26 can be seen that displacements near the hanging wall side of the open pit, half of displacements are vertical and half are horizontal. Further from open pit the displacements are, more it will be oriented horizontally. Rectangles figures are 500 meters wide and – long.

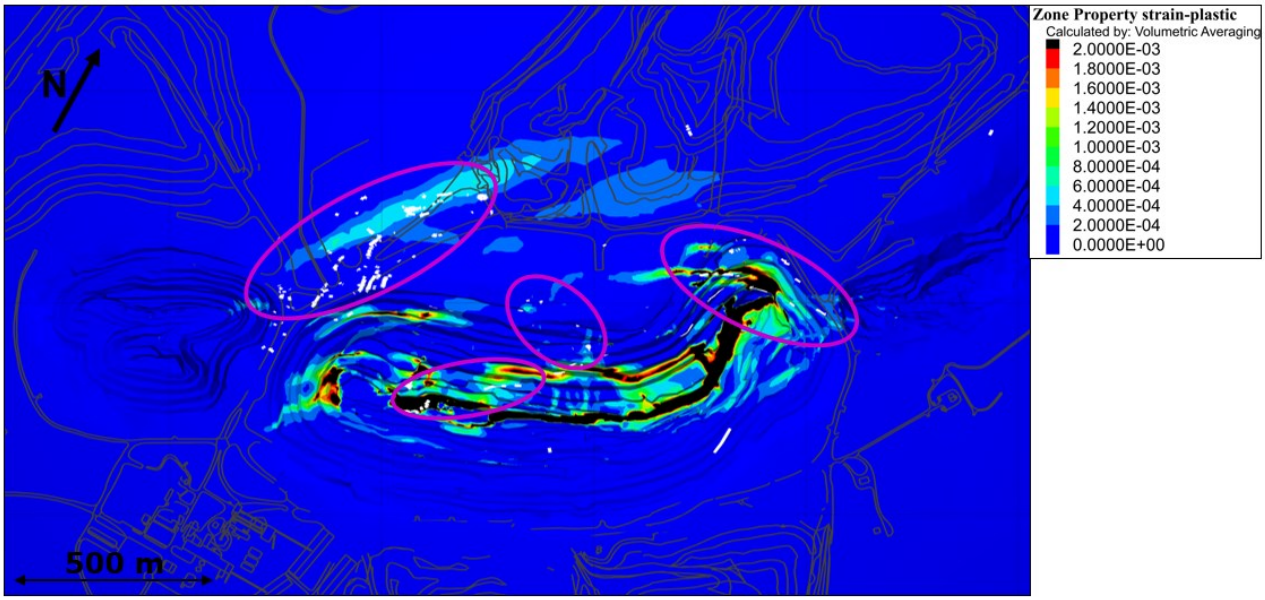

Figure 24 Starting plastic strain state for the simulations on the surface, observed cracks from the mine as white dots and -lines. Areas within magenta ellipses contain many cracks.

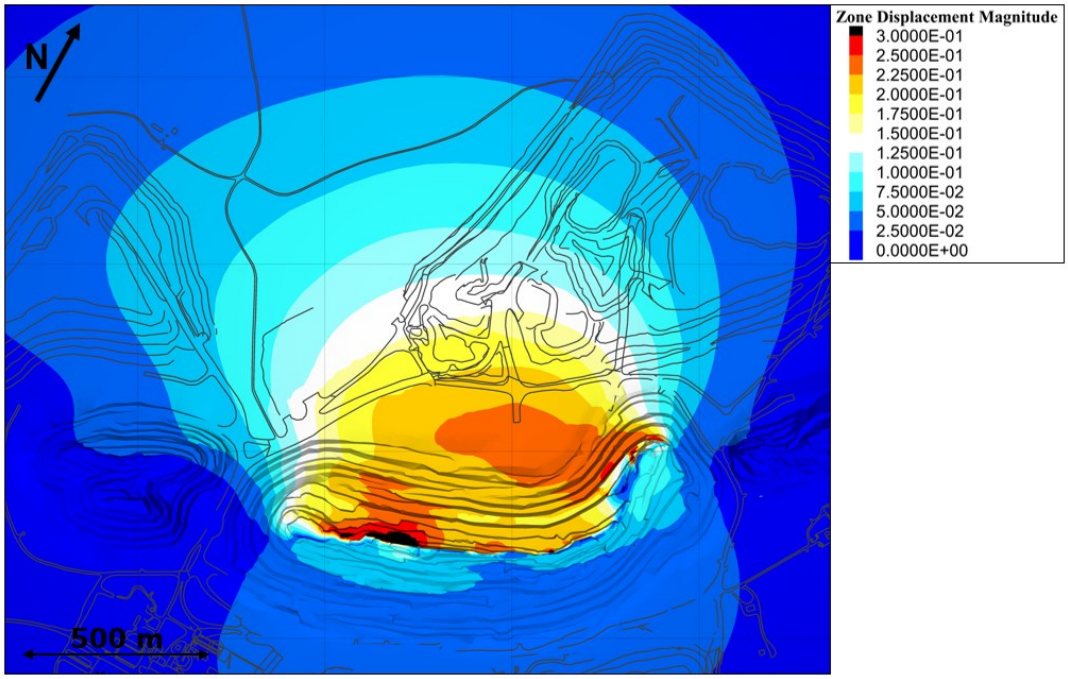

Figure 25 Starting total displacement state for the simulations on the surface

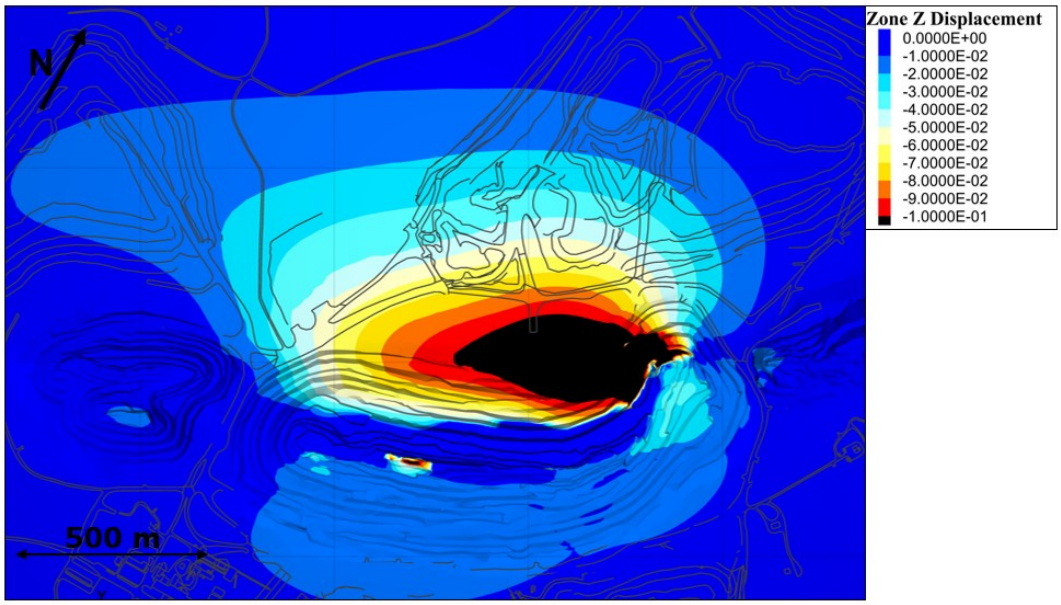

Figure 26 Starting vertical displacement state for the simulations on the surface

5.1 Global stability of UGB with fill simulations (S0)

Scenario where everything is excavated using UGB will be used as a base comparison scenario for all the other scenarios. As SLC method isn't used in any mining area, plastic stains and displacements should be small or moderate.

After Deep I has been mined, existing plastic strains on surface grows in magnitude and area. Also completely new plastic strain areas form on ground surface as can be seen from Figure 27. The most notable plastic strain areas are at the northern side of ELPV open pit, across SO open pit and between SO and EL open pit. In these areas can be seen higher plastic strains than $20e^{-4}$ (0,20%).

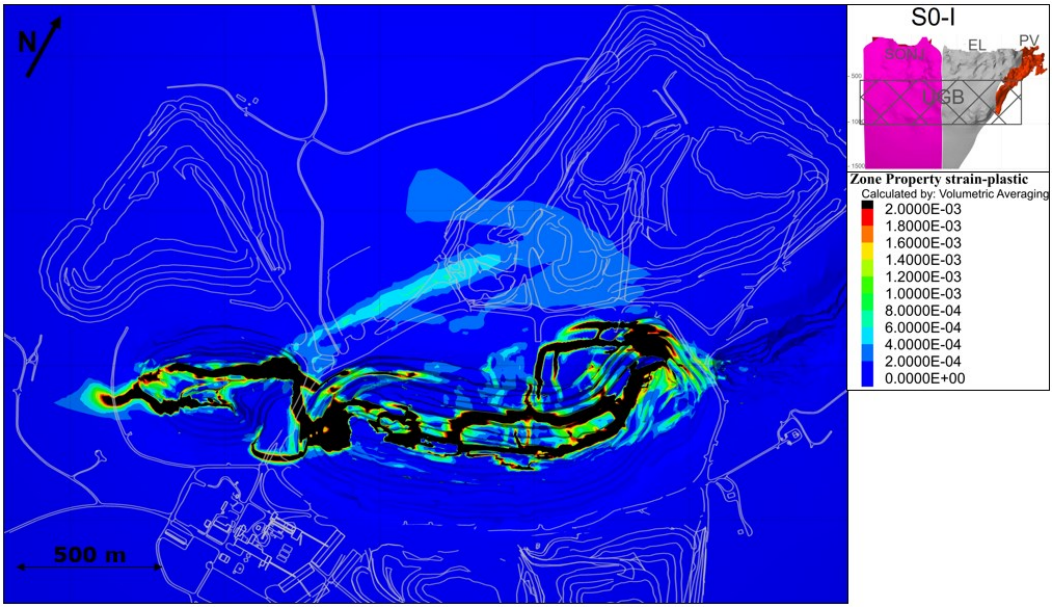

Figure 27 Plastic strain on the surface after Deep I has been excavated in scenario 0

Mining of Deep I causes at the surface total displacements of 20 cm in magnitude to expand at the hanging wall side to around 1000 meters away from the open pits. This is shown in approximately 800 meters further than the present state is. Total displacements are shown at the Figure 28. By comparing total displacement figure to the plastic strain – and vertical displacement figure, can be deduced that total displacements are orientated at the surface heavily horizontally and are elastic. Vertical displacements at the surface are presented in Figure 29.

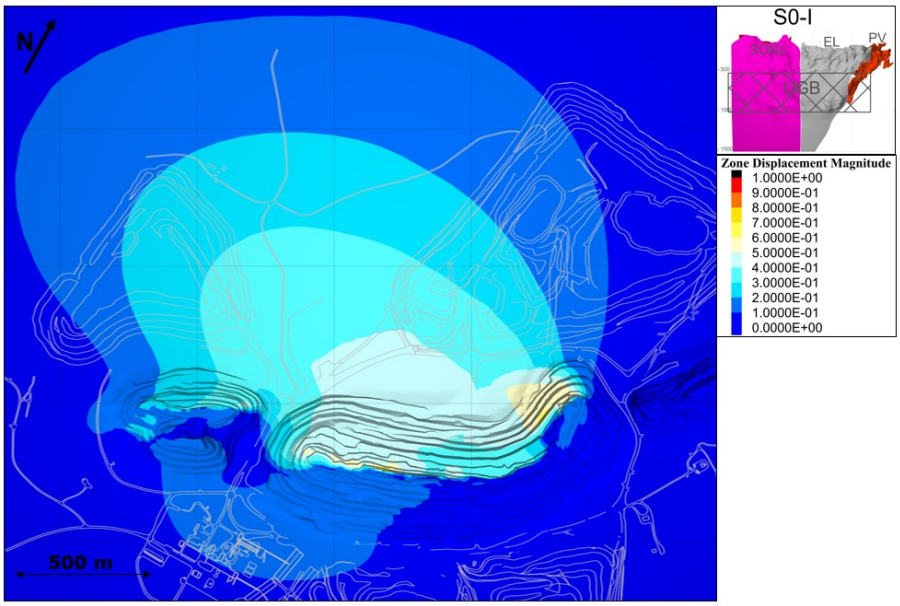

Figure 28 Total displacements on the surface after Deep I has been excavated in scenario 0

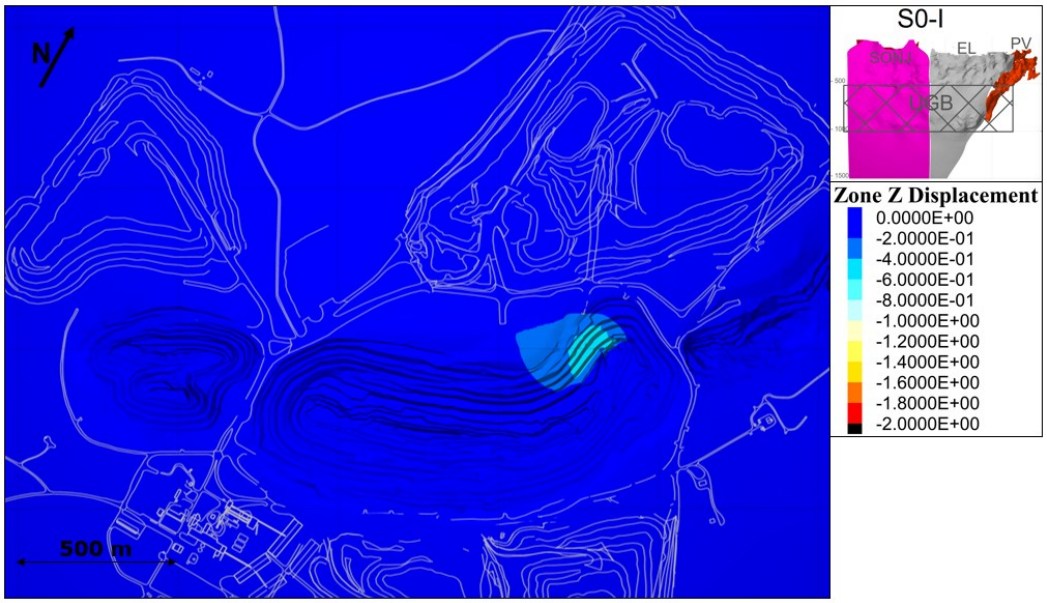

Figure 29 Vertical displacements on the surface after Deep I has been excavated in scenario 0

After Deep I, the Deep II is mined and mining induced strains and displacements grow. Plastic strains at the surface after the Deep II has been mined are represented in Figure 30. From this figure can be noticed, that into addition of growth of old cracks shown in the Figure 24, new cracks at the surface starts to form between pre-existing long crack failure

area and north-eastern side of ELPV open pit. Also a small new crack area forms near to the western side of SO open pit.

Total- and vertical displacements are illustrated in Figure 31 and Figure 32. Total displacements of 40 cm now extend from open pits 1000 meters away. Again the displacements are orientated heavily horizontally.

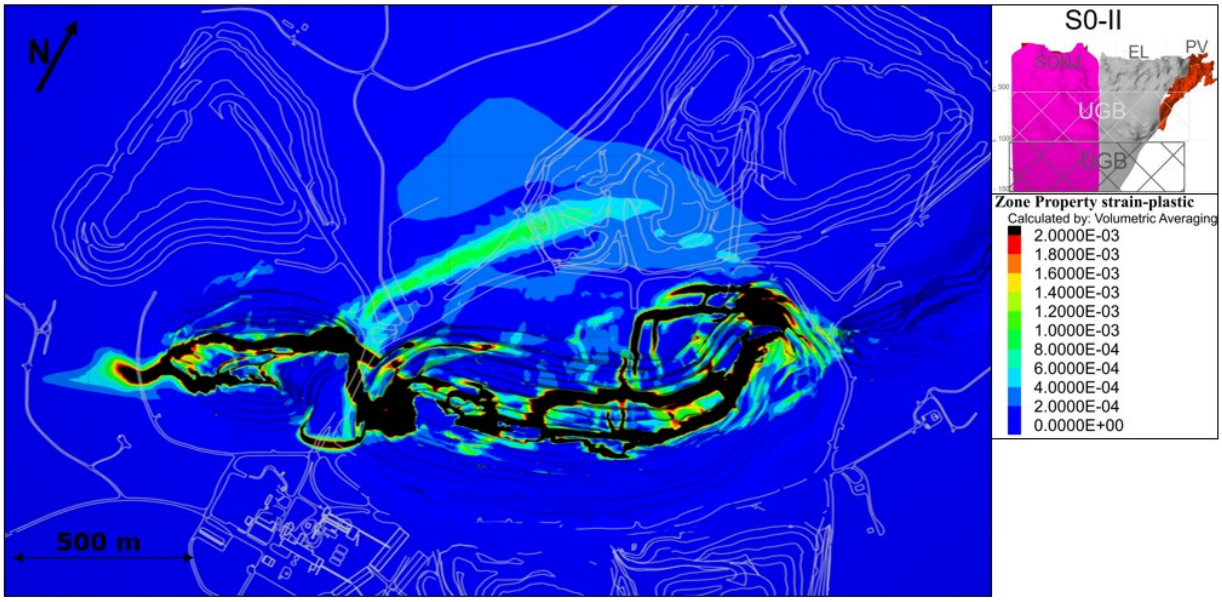

Figure 30 Plastic strain on the surface after Deep II has been excavated in scenario 0

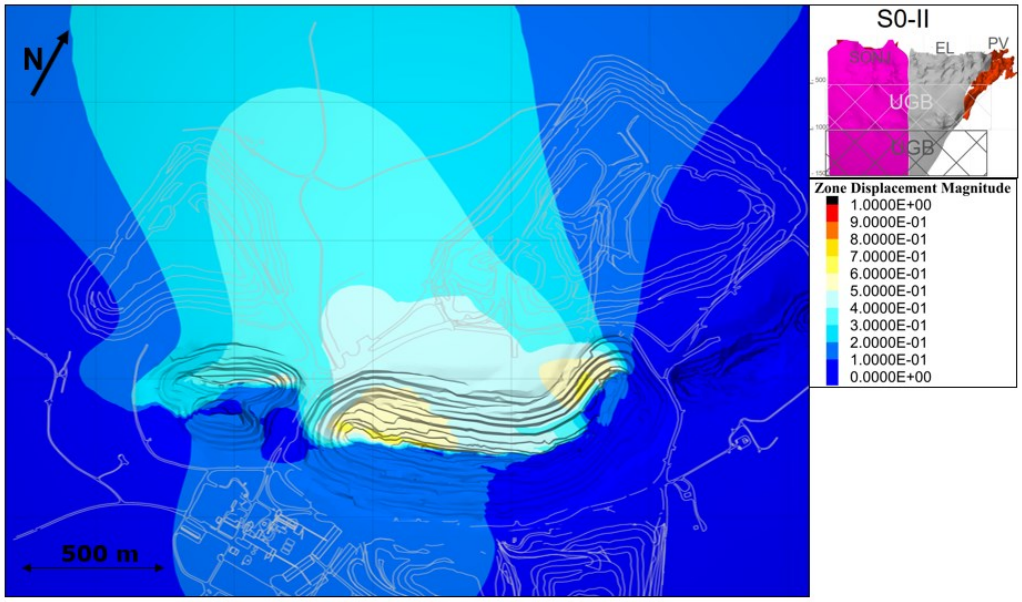

Figure 31 Total displacements on the surface after Deep II has been excavated in scenario 0

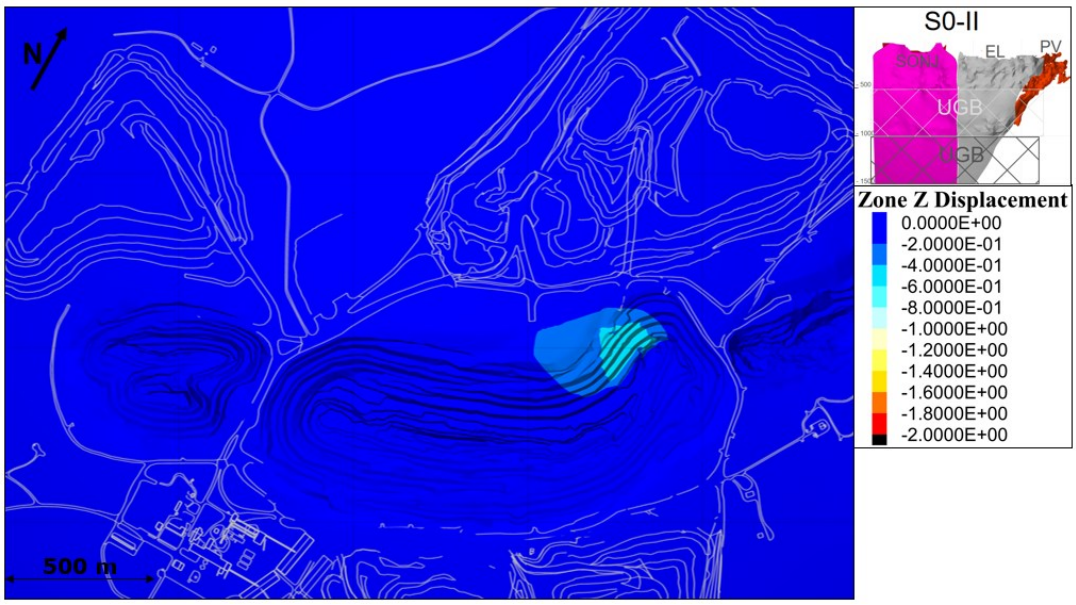

Figure 32 Vertical displacements on the surface after Deep II has been excavated in scenario 0

In conclusion, from the current state of the mine point when all mining areas are mined with UGB, the plastic strain and displacements have grown noticeable amount whereas there is only a slight change in vertical displacements. New cracks at the surface near PV-side of ELPV- and SO open pit are formed in addition of expansion of the currently present cracking areas.

5.2 Global stability of SLC simulations (S1)

As all the excavations after the current mine are excavated using SLC in scenario one, changes in the plastic strains and displacements are bigger than in scenario 0. After Deep I has been mined, plastic strains at the surface can be seen from Figure 33. As in scenario 0, new cracking areas forms at the SO open pit and it's near vicinity. In addition of that, aforementioned cracking area extend from SO open pit to another new cracking area around 500 meters away from the open pits at the hanging wall side. This new area where cracks are forming is nearly 400 meters wide and 1000 meters long. These areas results in to an arch of cracking areas from the North-Western side of SO open pit to the North-Eastern side of ELPV open pit.

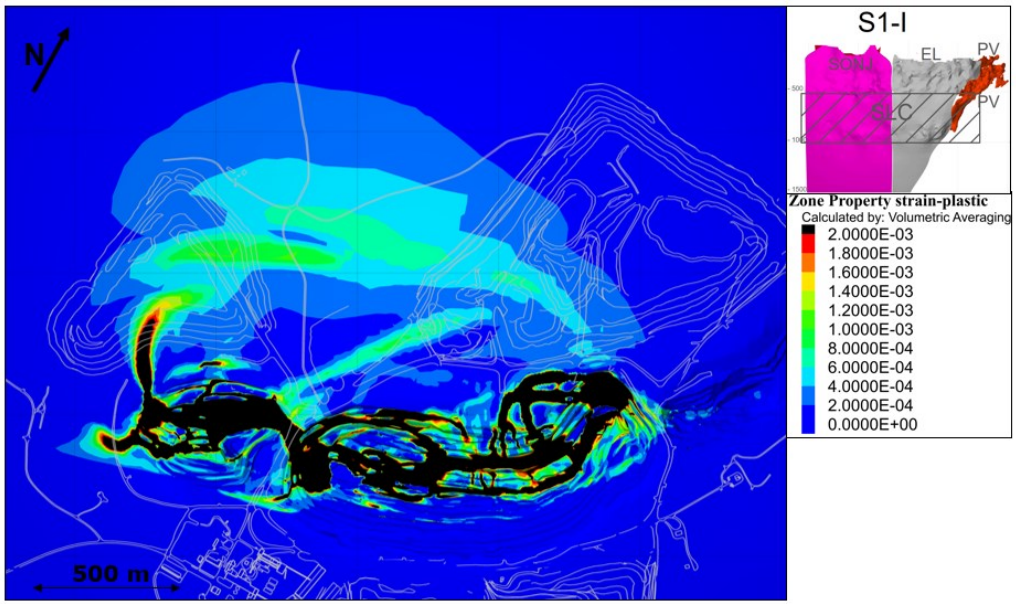

Figure 33 Plastic strain on the surface after Deep I has been excavated in scenario 1

At the surface displacement magnitudes range from the open pit subsidence areas of greater than 1 meter of total displacements to the 10 cm of total displacements 1500 meters away from open pits. Huge displacements are focused at the middle of hanging wall side of SO-, EL- and PV open pits. From the SO- and EL open pit. By inspecting both of total- (Figure 34) and vertical displacements (Figure 35) can noticed that, displacements are mainly horizontal with exception being areas with more than 80 cm of total displacements. At the outer edges of these areas the magnitudes of vertical and horizontal displacements are equal and closer the center of huge displacement areas the higher the vertical displacements are compared to the horizontal displacements. The magnitude of displacements and plastic strains indicate that within areas of huge displacements surface subsidence can already be close to cratering.

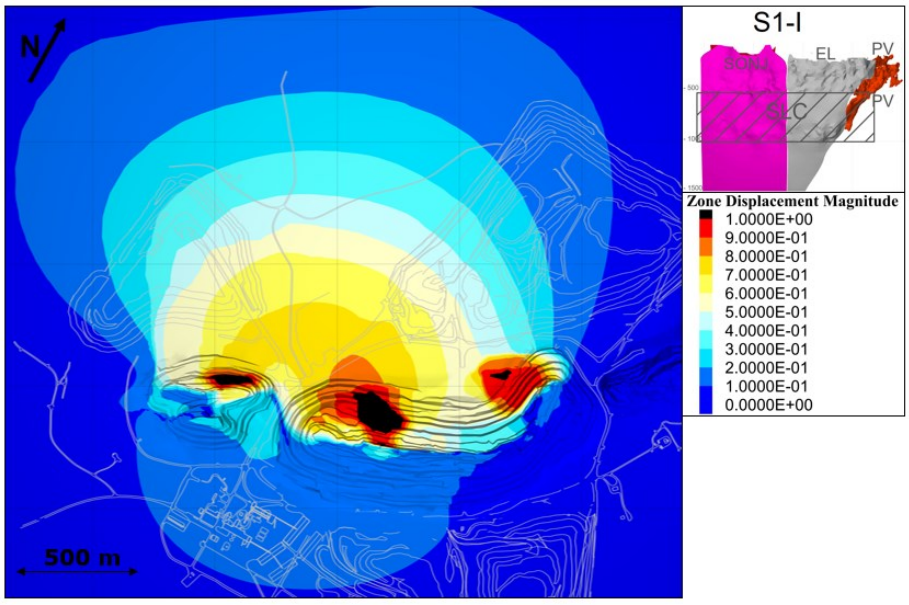

Figure 34 Total displacements on the surface after Deep I has been excavated in scenario 1

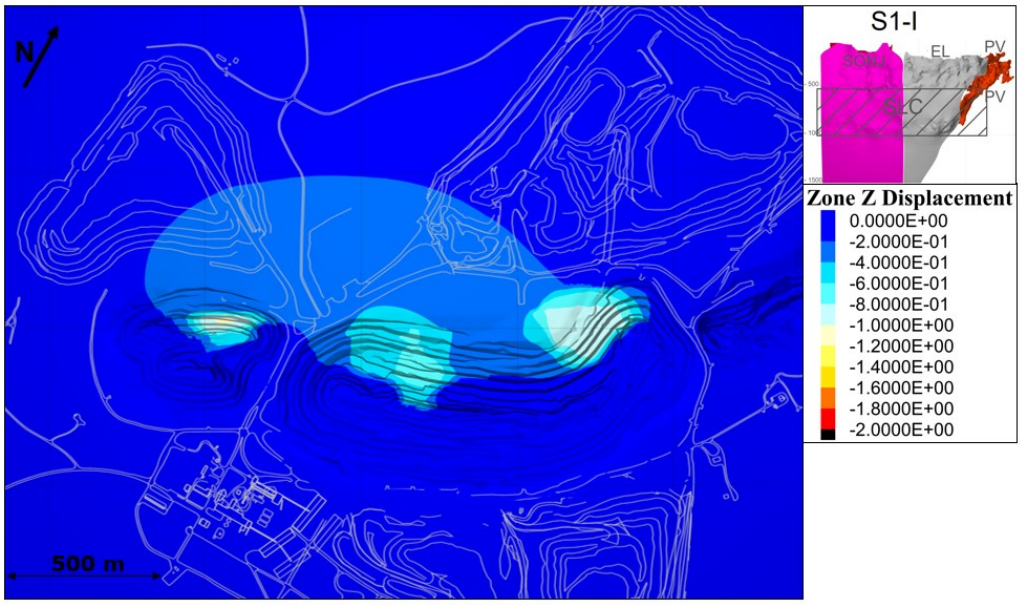

Figure 35 Vertical displacements on the surface after Deep I has been excavated in scenario 1

When the whole mine has been mined with SLC-method, plastic strain areas with magnitude over $4e^{-4}$ have extended over 1100 meters from the open pits and earlier cracking areas grow in size and magnitude. Considerable grow occurs in areas of earlier surface subsidence and can now be interpreted evolved into surface cratering in SO- and EL areas (Figure 36).

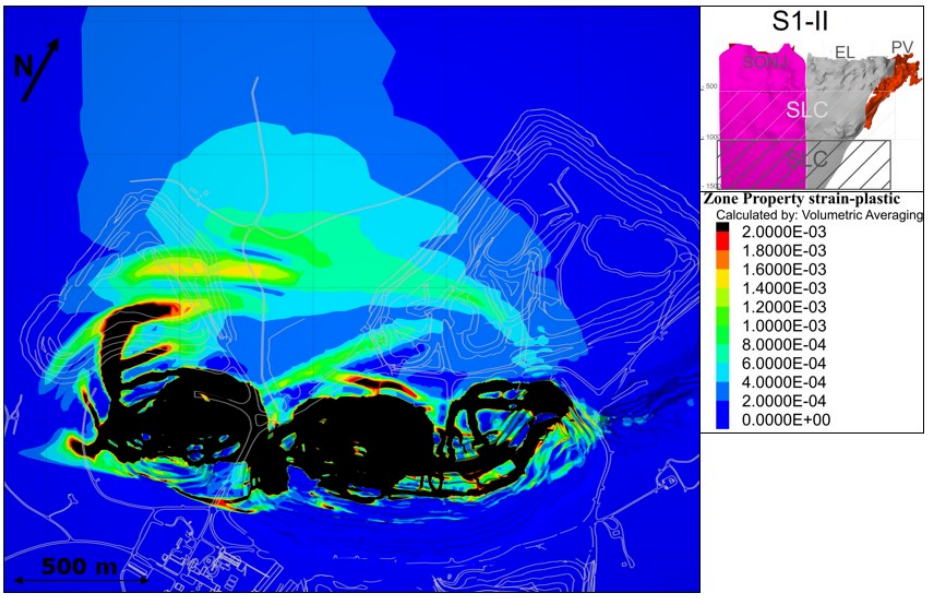

Figure 36 Plastic strain on the surface after Deep II has been excavated in scenario 1

Over 1 meter displacements areas of SO- and EL will connect to each other during mining of the Deep II. Displacements higher than 30 cm now extend 1250 meters from open pits and area with displacements of 20 cm almost reaches infrastructure at the footwall side (Figure 37). Displacements are primary horizontal outside SO- and EL cratering areas, which can be easily seen as black areas from Figure 38. From the same figure can be noticed that vertical displacements grow rapidly in magnitude after exceeding 80 cm in SO- and EL open pits.

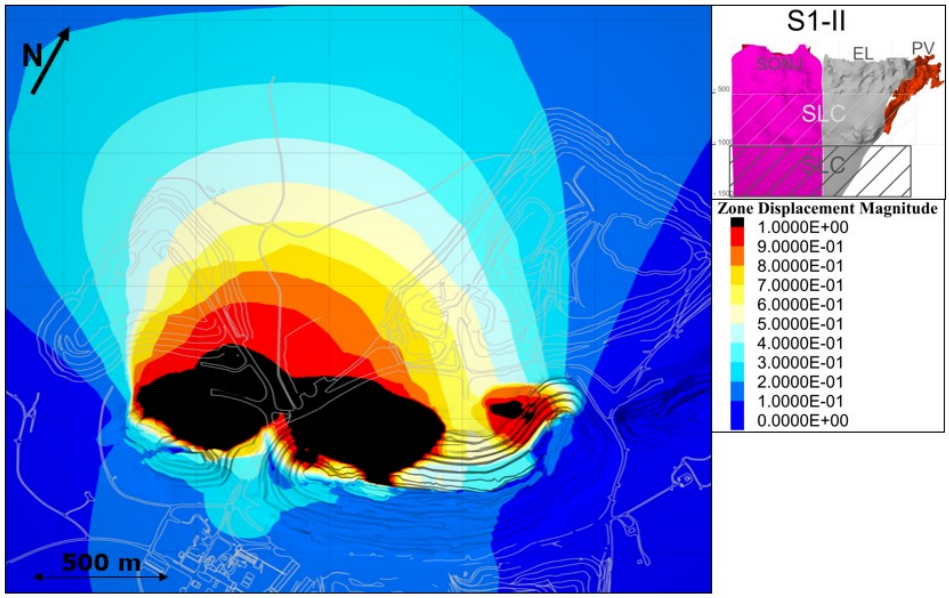

Figure 37 Total displacements on the surface after Deep II has been excavated in scenario 1

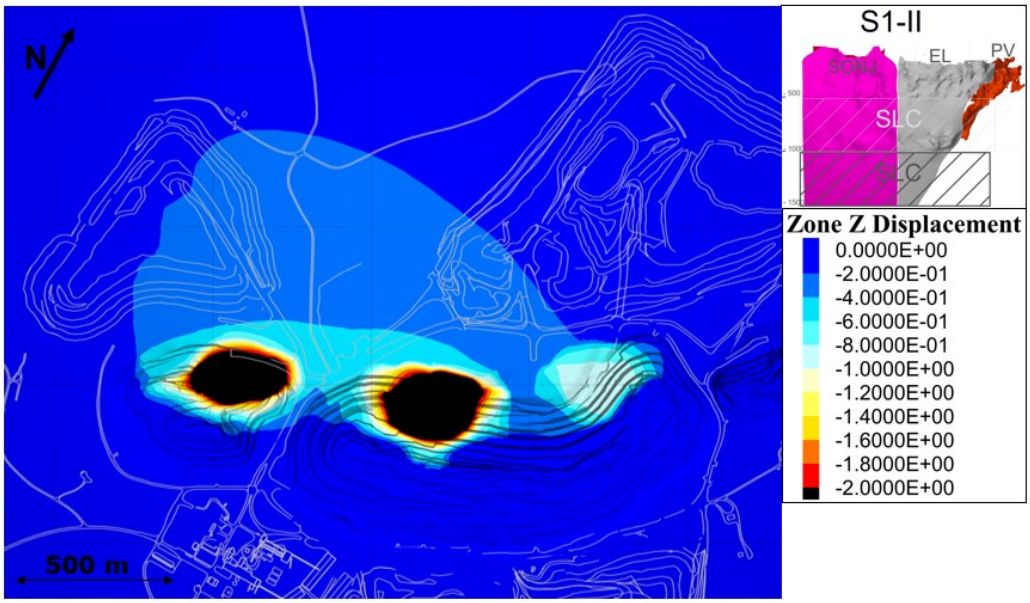

Figure 38 Vertical displacements on the surface after Deep II has been excavated in scenario 1

5.3 Global stability of combination simulations (S2&S3)

In this chapter results from scenarios 2 and – 3 are represented in ascending order. As the mine excavated using both UGB- and SLC- methods, the magnitude and size of strains- and displacements will be between scenarios 0 and -1.

By first mining levels – 950 to -825 with UGB and then levels above level -825 with SLC, new cracking areas are formed on North-Western direction from SO open pit. Closer one of these areas is around 50 meters and the further one 550 meters away from SO open pit.

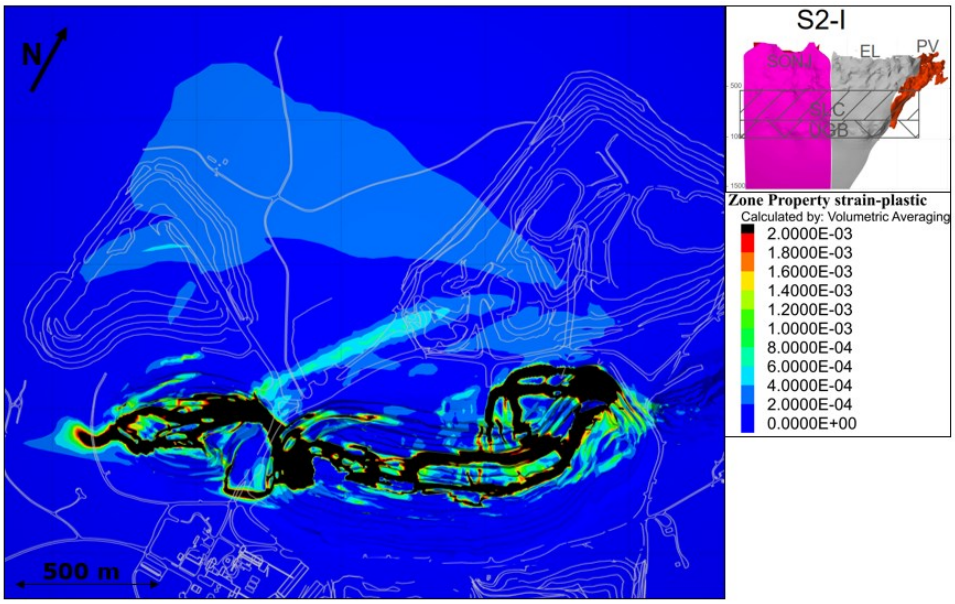

Figure 39 Plastic strain on the surface after Deep I has been excavated in scenario 2

Displacements are focused on the hanging wall side of PV-, EL and SO open pits. These displacements are inclined more horizontally than vertically and are over 50 cm in magnitude. Total displacements are shown in Figure 40 and vertical displacements in Figure 41.

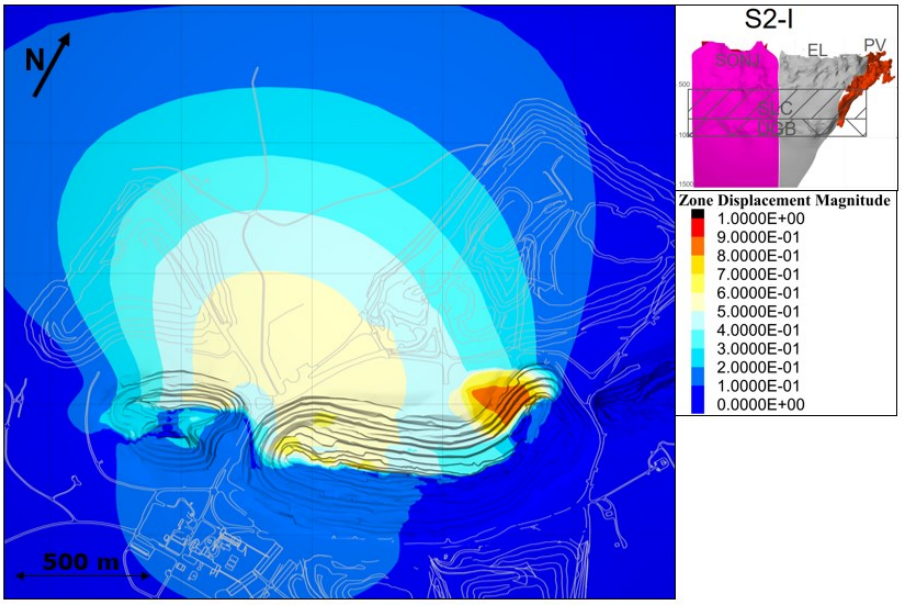

Figure 40 Total displacements on the surface after Deep I has been excavated in scenario 2

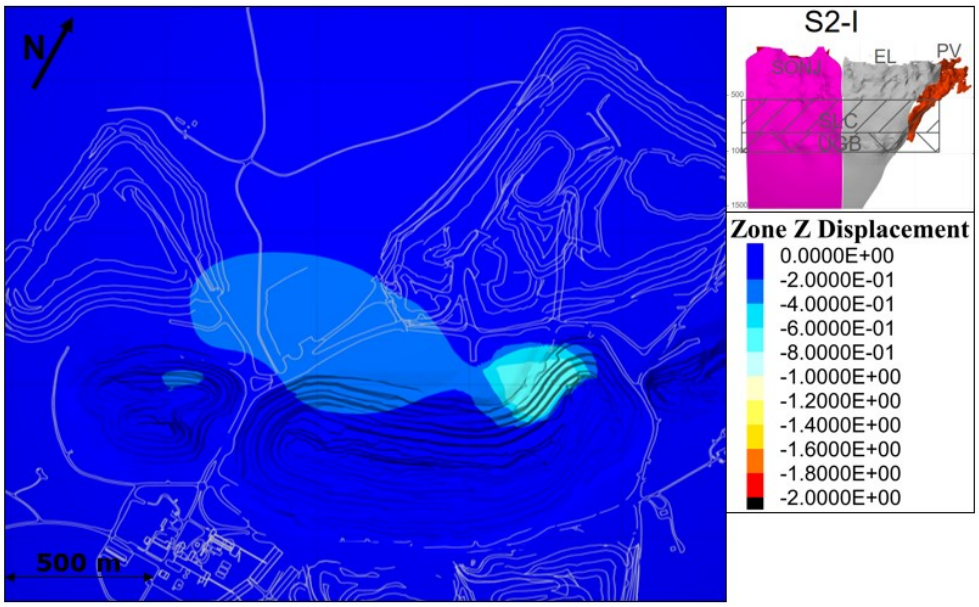

Figure 41 Vertical displacements on the surface after Deep I has been excavated in scenario 2

When excavating the Deep II, the caving will reach the bottom of back fill and upper caved rock area. Then the back fill and caved rocks will start to caving or fall down to the caving are created Deep II SLC-mining. This will change the caving from the Deep II levels to the upper part of Deep I and thus greatly affect to plastic strain on ground surface. UGB levels in the Deep I acts as a buffer zone between Deep I and -II SLC mining areas as there is less empty space available for the rock to cave in than in scenario 1.

After all mining areas have been excavated in scenario 2, plastic strains on the surface are focused heavily from the East- to North side of the hanging wall side near SO open pit and 500 meters away from open pits. Also cracking zone induced during mining of the Deep I at the foot wall side of the South-Eastern part of SO open pit continues to expand towards South and East. It also connects to the new large failure area at the North-Eastern side of SO open pit. These plastic strains are illustrated in the Figure 42 below.

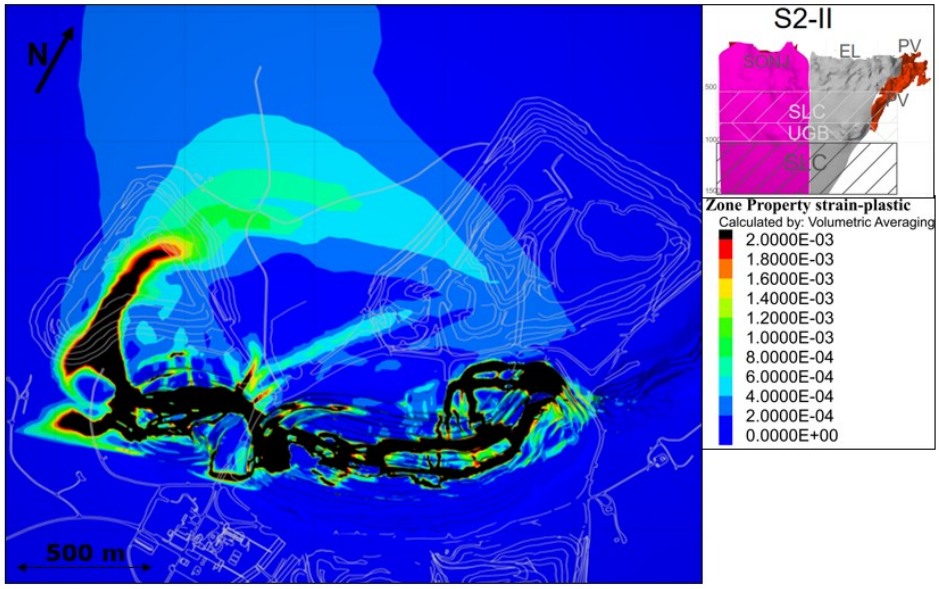

Figure 42 Plastic strain on the surface after Deep II has been excavated in scenario 2

Displacements on the surface are also higher in magnitude at the SO open pit side of the model than in EL open pit side. Total displacements (Figure 43) exceed 1 meter At the North-Eastern part of SO the open pit and near open pits it increases from Deep I mining induced 50 cm to 70 cm. Also there is small increase in magnitude and – area at the hanging wall side of the PV side of ELPV open pit. Displacements of 30 cm or higher reach out to around 1300 meters away open pits. By comparing total displacements in Figure 43 and vertical displacements in Figure 44 can be deduced that, displacements are mainly oriented horizontal with PV area being exception. Displacements with magnitude over 50 cm at the hanging wall side of PV open pit are around 80-90 % vertical and 20-10 % horizontal, with the inclination becoming increasingly vertical as the displacements increase in magnitude. Also the rock wall separating SO- and EL open pits has total displacements of 20 cm at the footwall side.

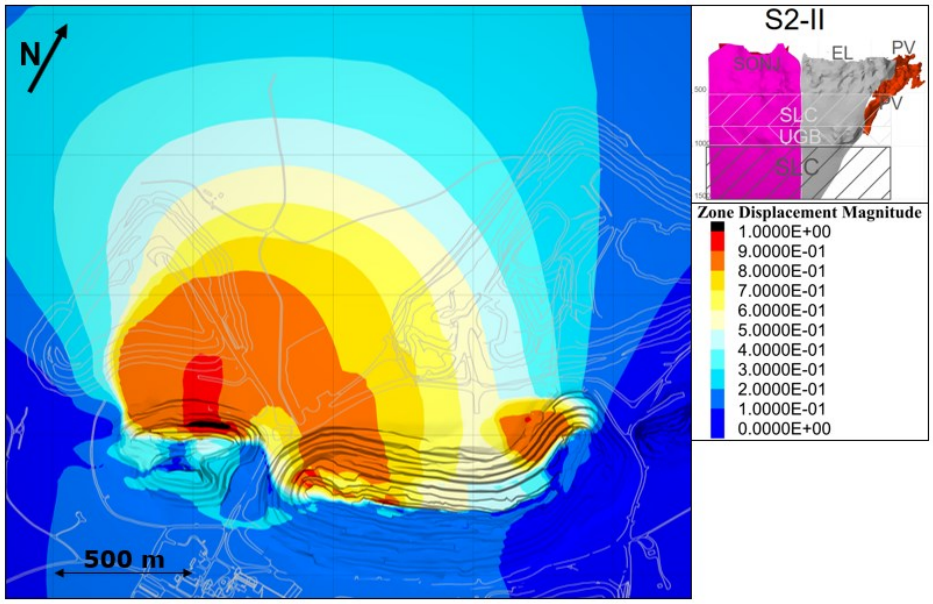

Figure 43 Total displacements on the surface after Deep II has been excavated in scenario 2

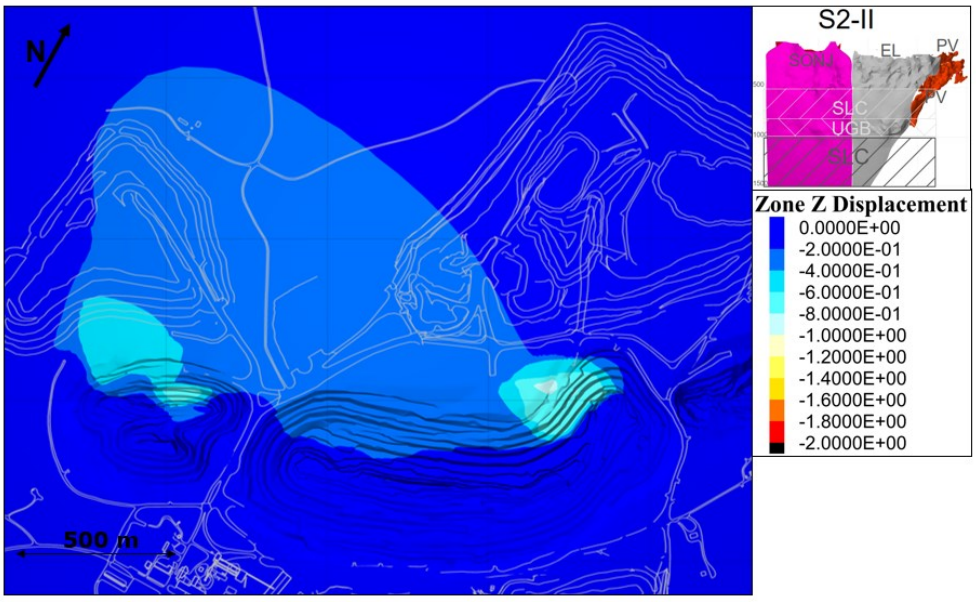

Figure 44 Vertical displacements on the surface after Deep II has been excavated in scenario 2

The other scenario containing both UBG- and SLC mining methods is scenario 3. In scenario 3 whole EL Deep I mining area is excavated with UGB and rest of the mine with SLC mining. Thus UGB- and SLC mining are divided by orebody and depth. Where as in scenario 2 UGB- and SLC mining divided by depth (mining levels) instead. As such strains and displacements should focus on the SO side of the mine, where the whole ore body is excavated with SLC mining.

After excavating Deep I in scenario 3, existing plastic strains on the surface grow expectedly in magnitude and size as shown in Figure 45. Differences between SO and EL mining areas can be observed as in addition of plastic strains near open pits increase, new plastic strain areas start to develop around 700- and 1000 meters away from SO open pit.

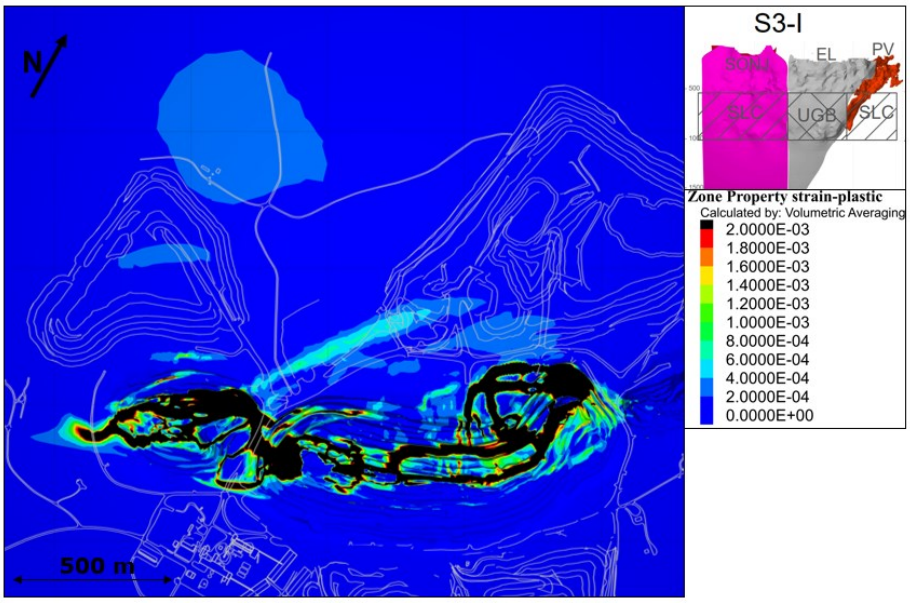

Figure 45 Plastic strain on the surface after Deep I has been excavated in scenario 3

Same trend of SO being more active side of the model in scenario 3, can be observed by examining displacements on the surface. Total displacements shown in the Figure 46 are focused at the PV side of the model. There is 10 cm difference in magnitude of total displacements between SO- and EL open pit's hanging wall sides. Total displacements contours slightly lean towards North-West. Around 350 meters away from open pits there is area in the middle of over 40 cm contour with displacement magnitudes over 50 cm. This area is slightly more at the SO side of the mine and closer to EL open pit there is another smaller area with 50 cm or more total displacements. By comparing total displacements shown in Figure 46 to vertical displacements in Figure 47, can be noticed that those areas with 50 cm displacements are within area of vertical displacements of 20 cm or higher. Vertical displacements are most noticeable at the hanging wall sides of PV- and SO open pits, where the magnitudes exceed 40 cm.

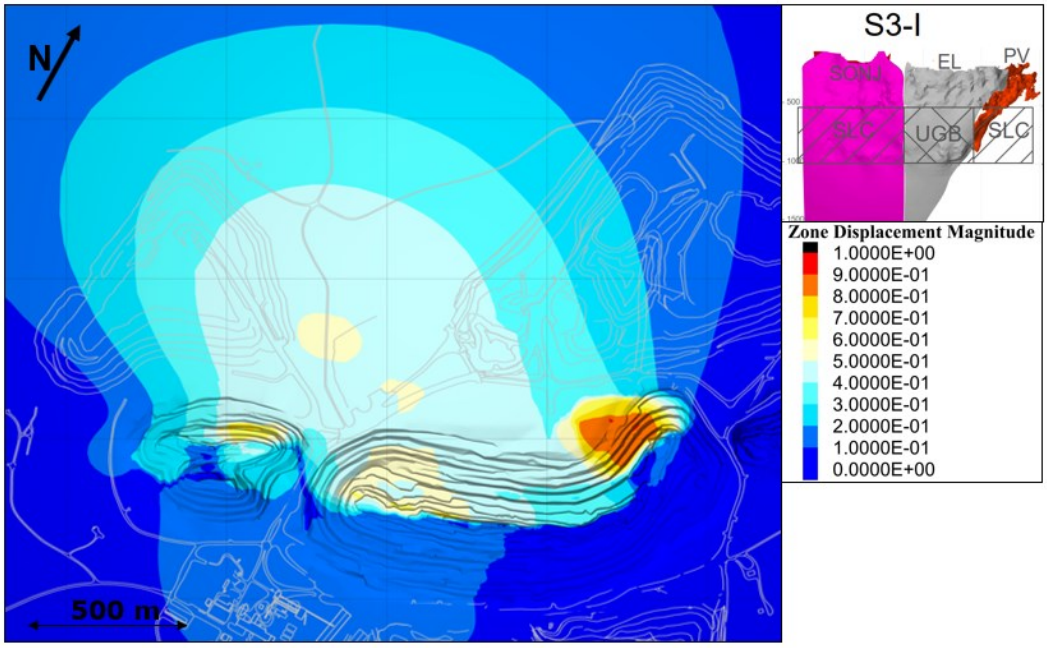

8

Figure 46 Total displacements on the surface after Deep I has been excavated in scenario 3

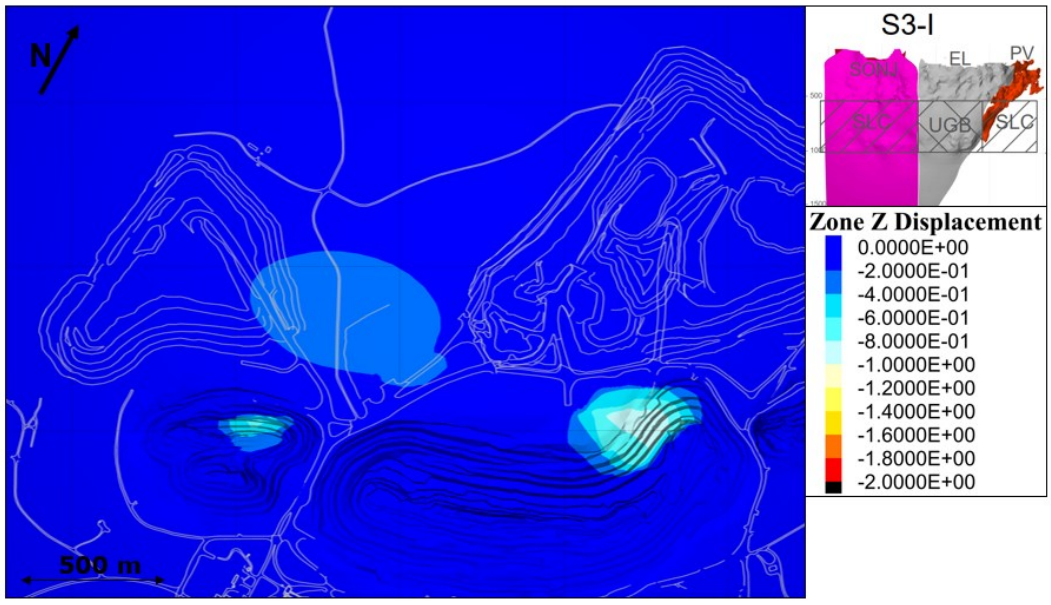

Figure 47 Vertical displacements on the surface after Deep I has been excavated in scenario 3

Once the Deep II has been mined with SLC method thorough out the mine, the plastic strains and displacements induced by mining of the Deep I enlarges. This enlargements reinforces the differences in magnitude- and area. This effect can be seen from the Figure 48, where the plastic trains between SO- and EL sides at the surface have significant difference in area and – magnitude. Whereas at EL side earlier cracking areas grow slightly, at the SO side new cracking areas forms from the western part of SO open pit as an arc shaped area to almost 800 meters away from open pits. Also new cracking arc are formed at the foot wall side of the SO open pit.

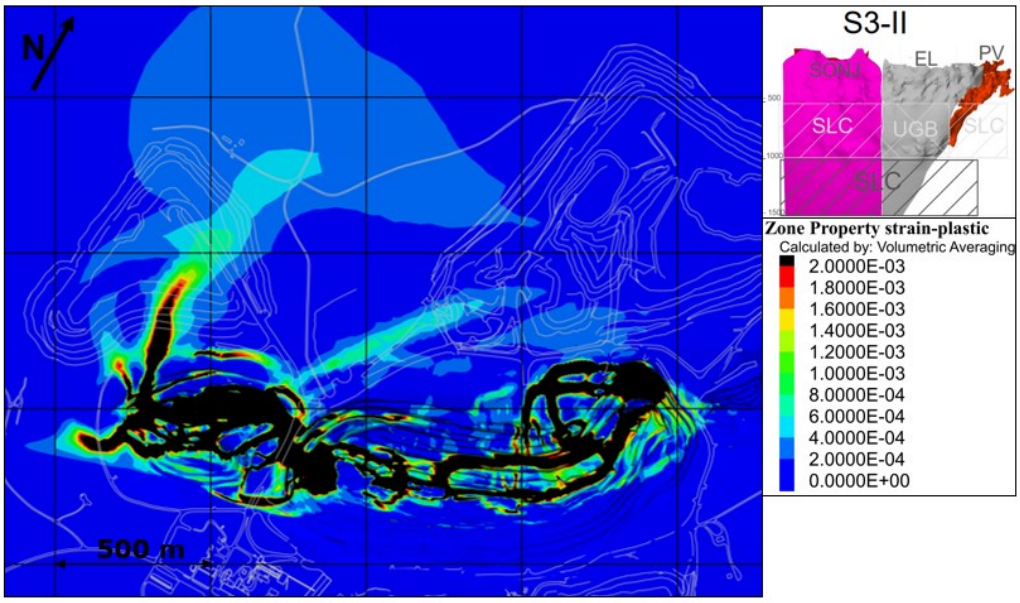

Figure 48 Plastic strain on the surface after Deep II has been excavated in scenario 3

Total Displacements shown in Figure 49 and vertical displacements in Figure 50 also illustrate the differences between SO- and EL sides. In both of the displacement figures for the end of the scenario 3, clearly show the area of active movement at the northern part of SO open pit, where vertical displacements exceed 1,8 meters. This can be interpreted as cratering of the hanging wall side and the black contour in the Figure 49 highlights the area of cratering.

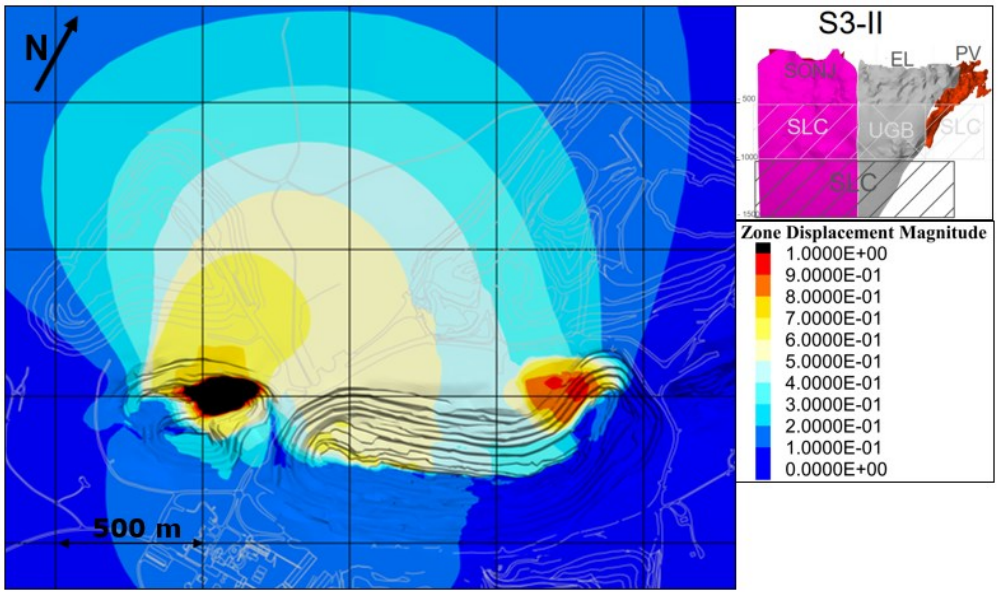

Figure 49 Total displacements on the surface after Deep II has been excavated in scenario 3

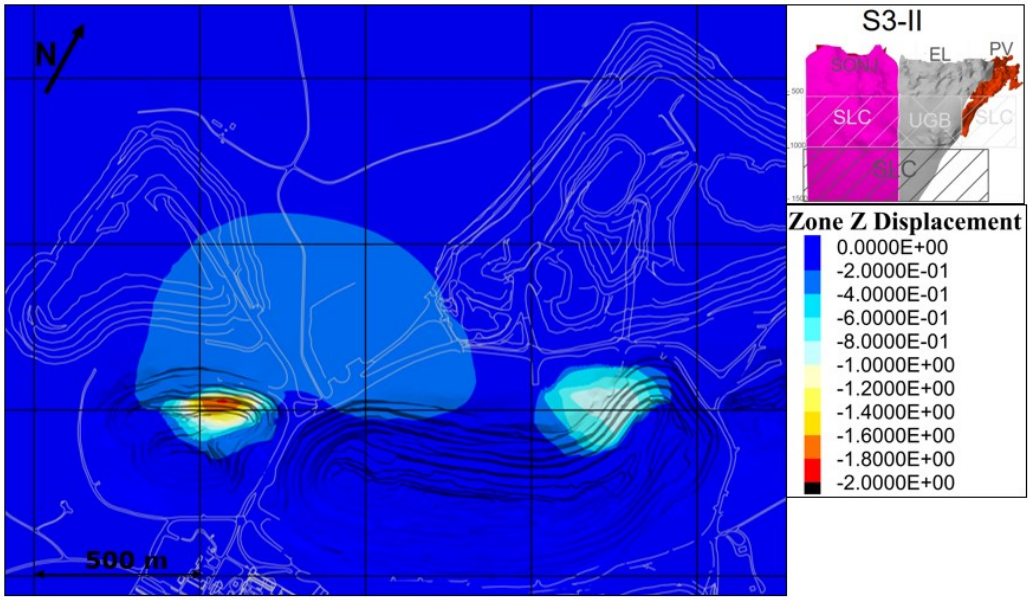

Figure 50 Vertical displacements on the surface after Deep II has been excavated in scenario 3

5.4 Reliability of results

Reliability of the results are lowered by many different kinds of factors. These factors range from larger errors such as wrong simulation logic to the very detailed errors, for example inaccurate geometries of small areas. In this thesis the results are first examined by whether the areas of change- and internal differences of magnitudes within the model are logical. This done to spot any critical flaws in the simulation logic and model building. Then the magnitudes of the results are examined and evaluated, to find if the used parameters work correctly with the simulation logic and – the model.

The simulated current state of the mine was calibrated to correspond the real state of the mine and as such eliminate errors in the simulation running code and the model building. As previously mentioned in chapter 4.3, the parameters for the metaperiodate were chosen based on parameter study done with calibration simulation model. The parameter study for the metaperiodate was also used to spot any problems in the model building, region settings and in-situ stresses.

Particularly the setting of the in-situ stress state to the model affected considerably to the results. This led to a problem as the ground surface on top of the model isn't flat, but slightly bends toward the open pits. In another words the elevation level where the in-situ stresses are zero can't be the elevation level zero. If the in-situ stresses would be assigned to be zero at the elevation level zero, the magnitude of in-situ stresses near open pits would be unrealistically high and such there would be more deformations near the open pits as there is in reality. During the parameter study of the metaperiodate also a study of in-situ stress was done, in order to find out, what elevation level should be assigned as the zero stress level for the in-situ parameter calculations. For the model used in thesis level -40 meters was chosen as the zero stress level. However, it's important to point out that even with the quite complex model geometries some rock types are absent from the model and thus not representing fully the complex geological environment within Kemi mine.

By conducting aforementioned parameter studies, a significant part of factors leading to inaccurate results were diminished. Removing all the inaccuracies in-situ state- and used material parameters is out of this thesis's scope as it would require rigorous back-calculations and parameter studies. As such the results to the simulated current state of the mine are fairly accurate and reliable within the scope of the thesis. The results obtained from the different simulation scenarios are discussed next.

Scenario 0 continues the from the current state of mine without any major change. The simulation logic is same as before (only UGB mining) and not whole mining levels are excavated as the Outokumpu Oy has provided preliminary stope excavation plans. The results for the first half of the scenario 0 are reasonable; the results show new failures around new excavations near ground surface in similar magnitude as earlier in other parts of the open pits and displacements grow and spread in logical manor within the model.

The stope plan doesn't reach as far in the Deep II than in the Deep I. If there is not either stope plan nor mining-limits area on the mining level, the whole level is excavated. This leads the latter half of scenario 0 to be less accurate mining wise than the current state and the first half of the scenario 0. As such the mining induced changes within the mine are overestimated. The magnitude of the overestimation depends solely on the executed mining plan and it degreases with increased mining out-side of the given stope plans for this thesis. This is also true for the rest of the scenarios, where the SLC-stope plan reach a bit further in the Deep II than the UGB-stope plan.

In short the results from the scenario 0 are fairly reliable for the current state of the mine (and such for all the other scenarios) and from the excavation of the Deep I. The Deep II results are on the conservative side as the strains and displacements are overestimated. Examining the reliability of the results for the rest of the scenarios is more difficult. This is due the SLC-mining within those scenarios.

Breaking of the bedrock to loose- and freely moving boulder is critical part of the SLC-mining logic. This taken into account with bulking factor. Bulking factor directly affects considerably to SLC-mining as the it determines the voracity of the caving. Lower value indicates less bulking and thus less supporting volume from the broken bedrock and vice versa higher value leads greater supporting volume from the same amount of broken bedrock. For this thesis, the used value for the maximum volume increase was taken from literature. In-situ data of different rock types from Kemi rocks' bulking factor would increase the accuracy of the SLC-simulations.

Another important aspect of the SLC-mining logic is the interpretation of the areas of free movement and the yielded zone above it. In the used SLC-simulation logic only cross-sections of active movement areas are taken into account when calculating supporting boulder areas. Firstly this excludes three dimensional aspect of the boulder movements within the cavern and thus not taken into consideration the real shape of the supporting boulder mass. Secondly in the simulation logic is assumed that there is no air gab between area of active movement and yielded zone. This slightly underestimates the amount of supporting boulder needed to stabilize caving and thus overestimating slightly yielding in the surrounding rock.

There is no reference data of the SLC-mining from the Kemi mine and the closets references of 3D SLC-caving simulations have been done with different software modules than for this thesis was possible to get. As such, the very SLC-mining logic sequence created in this thesis hasn't yet been verified and the interpretation of the results should be done critically.

Even though one should be critical towards exact results of the scenarios containing SLC-simulations, the overall magnitudes of the simulated SLC-mining induced plastic strains are reasonable. Also the direction displacements are growing and towards to are reasonable. Thus results from SLC-simulations can be used to carefully interpreted the directions- and scale of consequence's magnitude.

Aforementioned flaws in the SLC-simulation logic in addition with the unrealistic excavation sequence within mining levels discussed in chapter 4.4.2, impact the scenario 1 the most since in it practically whole mine is excavated with SLC-simulation logic. Thus from the known inaccuracies can be stated that scenario's 1 results are the most overestimated and the most affected by considerable unreliability factor of bulking factor. Also both the overestimation and error from bulking factor increases as the SLC excavation increases thus Deep II results are even more unreliable in scenario 1 than in 0.

In scenario 2 the errors from SLC-simulation are lowered with buffering zone created by UGB-mining and no-mining levels between SLC-mining in Deep I and – II. There is still overestimation of the results and considerable unreliability from bulking factor. Results from scenario 2 are more reliable than from scenario 1 and less reliable than from scenario 0.

Unreliability of the results from scenario 3 differs from other scenarios in one major way. As the UGB- and SLC mining are not only with mining levels but also with mining areas (ore bodies). This causes the SLC-mining focused areas of the model to be more unreliable than the mixed UGB- and SLC-mining area. Meaning that the plastic strains and displacements in the middle of the model (EL area) in scenario 3 are more reliable than on the sides of the model (SO- and PV areas).

In summary results from scenarios start as quite reliable due parameter calibration and become increasingly more unreliable as the mining continues within scenarios. Also the unreliability grows with increasing presence of SLC-mining. Thus results from the middle of scenario 0 are the most reliable results in this thesis when excluding the results from simulated current state of the mine. And the most unreliable results are from the end of scenario 1.

5.5 Comparison of the results between mining methods

Results from different scenarios vary a lot in terms of magnitude, area and reliability. Scenario 0 has expectedly the least mining induced strains and -displacements due lack of SLC-mining. Scenarios 2 and -3 have noticeably higher strains and -displacements than scenario 0. Also in scenarios 2 and -3 strains- and displacements are focused on the SO side of the mine, where as in scenario 0 displacements and mostly strains are greatest in magnitude at the center of the EL area of the mine. Main differences of the results from scenarios 2 and -3 are at the SO- and EL areas on the surface. The end of scenario 2 has greater displacements than end of scenario 3 with one area being exception. This is the area

in SO open pit with humongous vertical displacements of over 1,5 meters. Scenario 1 has clearly the greatest magnitudes and the most widely spread of strains and displacements of all studied scenarios. Below is summary of the results represented in Table 9 .

Table 9 Summary of the results

0: Minimal 1: Some 2: Considerable 3: Massive	Plastic strains	Total displacements	Vertical displacements
S0	1	1	0
S1	3	3	3
S2	2	2	1
S3	1,5	1,5	2

Results on the SO- and PV sides of the model are almost as unreliable than results from scenario 1 as the whole SO- and PV sides are excavated with SLC mining. Results from Deep I around EL area are nearly as reliable than from scenario 0 and from Deep II a little bit more reliable than from scenario 2, but not as reliable than from scenario 0.

As the results and comparison of them show, changing the mining method from current UGB- to SLC- method, would likely to create humongous displacements and failure zones at the hanging wall side of the ground surface. If that is unacceptable state of the Kemi mine for the Outokumpu Oy, mixing the SLC- and UGB mining methods could increase ore extraction efficacy without creating as massive displacements and failure zones at surface as if everything would be mined with SLC-method. For all the studied scenarios strains- and the displacements were on the footwall side of the surface quite small in magnitude and area.

6 Conclusions

Results showed that if excavation of the ore bodies are continued with the current mining method of UBG, the mining induced strains and displacements are going to increase immensely from the current state of the mine. If SLC-mining is mixed with the UGB mining method, the effects of mining will grow considerably. However, the use of UGB-mining and supporting buffer levels within orebodies reduced the otherwise humongous affects from the SLC-mining to the mine. Changing mining method to solely SLC-mining would thus greatly affect the ground surface around mine. Due the unreliability's of the new SLC-simulation logic the results from scenarios 1-3 are indicative in nature.

Reliability of the results begin as fairly reliable due parameter calibration and become increasingly more unreliable as the mining continues within scenarios due inaccurate mining plans. Also SLC-mining reduces unreliability of the results as the amount of SLC-mining increases meaning that, scenario containing mainly SLC-mining (scenario 1) has the most unreliable results in this thesis. By following aforementioned factors to the reliability of the results can be concluded that, results from the middle of scenario containing only UGB-mining (scenario 0) are the second most reliable results in this thesis, after the simulated current state of the mine.

From the results can be indicatively interpreted that if large displacements and surface cracking are acceptable within 1000 meters of the open pits, changing solely to SLC-mining could be possible. If not, then more precise simulations of mixed mining of UGB- and SLC-methods could meet the acceptable limits of strains- and displacements on the surface. This thesis's results indicate that on the surface the footwall side is only slightly affected by SLC-mining, compared to the hanging wall side. The worst-case scenario rock mechanical stability wise is scenario 1 where, hanging wall sides of open pits at the Surmaoja and Elijärvi areas will be center of cratering, meaning vertical displacements over two meters in magnitude. The best-case scenario rock mechanical stability wise is scenario 0, where is no cratering and mining induced visible deformations at the surface don't expand further than 50 meters from the existing failure areas.

7 Recommendations

During simulations and -writing this thesis, couple ways of improving of the used SLC-simulation logic and caving simulations to the Kemi mine have emerged. The SLC-simulation logic had two major unreliability factors of the bulking factor and the interpretation of the caving area. Also one way to improve the SLC-simulation logic significantly would be transition the interpretation of the caving areas from 2D cross-section areas to 3D volumes. Due the limited time for the thesis, a sensitivity analysis wasn't conducted even though it would greatly increase the knowledge of the reliability of the simulations. If this SLC-simulation logic is used, it is highly recommended that the aforementioned issues are addressed.

As for the recommendations specially for the Kemi mine, it is recommended to use the simulation results as an indicative information due the aforementioned factors in the chapter 5.4. Thus further caving simulation analyses are recommended to gain more accurate- and reliable results as well as the sensitively of the results.

These further analyses are recommended to be simulated using the latest modules and -version of the used software FLAC3D for caving analyses. For this thesis it was not possible to get latest caving simulation tools that were still in the developing phase. However, when this thesis is published, ITASCA CO. has introduced new constitutive model named "The Itasca Constitutive Model for Advanced Strain Softening" or IMASS in short. It is to the tailored needs of the complex caving simulations. Thus further caving analyses are recommended to conducted using IMASS and CAVESIM algorithm. Also it is recommend to test the sensitively of the simulation of aforementioned simulations with different parameters. It also would be interesting to examine how other caving methods used in mining would compare to the chosen alternatives and current method.

As the caving simulations get increasingly more complex, the required time to reach reliable- and accurate results increases. Thus, it is recommended to maintain the simulation goals and -model sizes moderate. The idea of having a simulation that addresses every points of interests at the same time can be tempt full. However, it can easily lead to poor simulation time and accurate results efficacy.

References

Brady, B.H.G & Brown, E.T. 2005. Rock mechanics for underground mining third edition, eBook ISBN: 1-4020-2116-X, Print ISBN: 1-4020-2064-3

Cai, M. et al. 2004. Estimation of rock mass strength and deformation modulus of jointed hard rock masses using the GSI system. Int J Rock Mech Min Sci (2004) 41(1):3–19.

Cai, M. et al. 2007. Determination of residual strength parameters of jointed rock masses using the GSI system. International Journal of Rock Mechanics and Mining Sciences. 44: 247-265. 10.1016/j.ijrmms.2006.07.005.

Cai, M. 2010. Practical Estimates of Tensile Strength and Hoek–Brown Strength Parameter mi of Brittle Rocks. Rock Mech Rock Eng (2010) 43:167–184
DOI 10.1007/s00603-009-0053-1

Duplancic, P. & Brady, B.H.G 1999. Characterisation of caving mechanisms by analysis of seismicity and rock stress. Proc. 9th Congr., Int. Soc. Rock Mech., Paris (eds G. Vouille and P. Berest), 2: 1049–53. A. A. Balkema: Rotterdam.

FLAC3D. 2017. FLAC3D6.0 Theory and Background. https://www.itascacg.com/software/downloads/flac3d-downloads

Hamrin, H. 2001. Underground mining methods and applications. Underground Mining Methods: Engineering Fundamentals and International Case Studies (eds W. A. Hustrulid and R. L. Bullock), 3–14. Society for Mining, Metallurgy and Exploration: Littleton, Colorado.

Huhtelin, T. 2015. The Kemi Chromite Deposit. In Maier, W.D., Lahtinen, R. & O'Brien, H. (Eds.) Mineral Deposits of Finland. Elsevier. pp. 165-178. ISBN 9780124104389.

Hoek, E. 2001. Rock mass properties for underground mines. Underground Mining Methods: Engineering Fundamentals and International Case Studies. (Edited by W. A. Hustrulid and R. L. Bullock), Litleton, Colorado: Society for Mining, Metallurgy, and Exploration (SME) 2001

Hoek, E. & Brown, ET. 2018. The Hoek-Brown failure criterion and GSI-2018 edition, Journal of Rock Mechanics and Geotechnical Engineering (2018), https://doi.org/10.1016/j.jrmge.2018.08.001

Hoek, E. & Diederichs M.S. 2005. Empirical estimation of rock mass modulus. International Journal of Rock Mechanics & Mining Sciences (2006) 43:203–215

Hoek, E. et al. 2002. Hoek-Brown failure criterion – 2002 Edition.

Rikberg, H. 2019. Field damage investigation and evaluation of numerical model using the collected data of Kemi mine. Master's thesis. Luleå University of Technology, Department of Civil, Environmental and Natural Resources Engineering

Sainsbury, B. 2011. A historical review of the development of numerical cave propagation simulations, in DP Sainsbury, RD Hart, CJ Detournary & MJ Nelson (eds), Proceedings of the 2nd International FLAC/DEM Symposium - Continuum and Distinct Element Numerical Modeling in Geomechanics, Itasca International Inc., Minneapolis, pp. 23–36.

Sainsbury, B. 2012. A model for cave propagation and subsidence assessment in jointed rock masses, PhD thesis, The University of New South Wales, Kensington, New South Wales

Salmi, J. 2018. Kemin kaivoksen syventäminen – DeepMine hanke, sited 29.5.2020, web material, available: https://www.lisaakauppaa.fi/file/download&file_id=264/

Sjöberg, J. et al. 2017. Deep sublevel cave mining and surface influence, in J Wesseloo (ed.), *Proceedings of the Eighth International Conference on Deep and High Stress Mining*, Australian Centre for Geomechanics, Perth, pp. 357-372, https://doi.org/10.36487/ACG_rep/1704_25_Sjoberg

Törmänen, J. 2019. Optimization of tunnel support in challenging rock conditions. Master's thesis. Aalto University, School of engineering. Espoo

Appendices

1) Appendix 1. mi table after Hoek. 2003
2) Mining order in scenario 0
3) Mining order in scenario 1
4) Mining order in scenario 2
5) Mining order in scenario 3

Appendix 1. mi table after Hoek. 2003

Rock Type	Class	Group	Texture			
			Coarse	Medium	Fine	Very fine
SEDIMENTARY	Clastic		Conglomerates* Breccias*	Sandstones 17± 4	Siltstones 7 ± 2 Greywackes (18 ± 3)	Claystones 4 ± 2 Shales (6± 2) Maris (7 ± 2)
	Non-Clastic	Carbonates	Crystalline Limestone (12 ± 3)	Sparitic Limestones (10 ± 2)	Micritic Limestones (9 ± 2)	Dolomites (9 ± 3)
		Evaporites		Gypsum 8 ± 2	Anhydrite 12 ± 2	
		Organic				Chalk 7 ± 2
METAMORPHIC	Non Foliated		Marble 9 ± 3	Hornfels (19 ± 4) Metasandstone (19 ± 3)	Quartzites 20 ± 3	
	Slightly foliated		Migmatite (29 ± 3)	Amphibolites 26 ± 6	Gneiss 28 ± 5	
	Foliated **			Schists 12 ± 3	Phyllites (7 ± 3)	Slates 7 ± 4
IGNEOUS	Plutonic	Light	Granite 32 ± 3	Diorite 25 ± 5		
			Granodiorite (29 ± 3)			
		Dark	Gabbro 27 ± 3	Dolerite (16 ± 5)		
				Norite 20 ± 5		
	Hypabyssal		Porphyries (20 ± 5)		Diabase (15 ± 5)	Periodotite (25 ± 5)
	Volcanic	Lava		Rhyolite (25 ± 5) Andesite 25 ± 5)	Dacite (25 ± 3) Basalt (25 ± 5)	
		Pyroclastic	Agglomerate (19 ± 3)	Breccia (19 ± 5)	Tuff (13 ± 5)	

*Conglomerates and breccias may present a wide range of m_i values depending on the nature of the cementing material and the degree of cementation, so they may range from values similar to sandstone, to values used for fine grained sediments (even under 10).

**These values are for intact rock specimens tested normal to bedding or foliation. The value of m_i will be significantly different if failure occurs along a weakness plane.

Appendix 2. Mining order in scenario 0

----------Mining order in scenario 0!----------Mining order in scenario 0!----------

Phase	ELPV,current mine, UGB	Start Level	End Level	SONJ, current mine, UGB	Start Level	End Level	ELPV,Deep-I mine, method	Start Level	End Level	SONJ, Deep-I mine, method	Start Level	End Level	ELPV,Deep-II mine, method	Start Level	End Level	SONJ, Deep-II mine, method	Start Level	End Level	
1	Pillar	225	200																
2	ELPV, UGB	500	475																
3	ELPV, UGB	475	450																
4	ELPV, UGB	450	425																
5	ELPV, UGB	425	400																
6	ELPV, UGB	400	375	SONJ, UGB	550	525													
7	ELPV, UGB	375	350	SONJ, UGB	525	500													
8	ELPV, UGB	350	325	SONJ, UGB	500	475													
9	ELPV, UGB	325	300	SONJ, UGB	475	450													
10	ELPV, UGB	300	275	SONJ, UGB	450	425													
11				SONJ+Horizontal-pillar	425	400													
12	Horizontal-pillar	400	375	SONJ, UGB	400	375	PLOT-RESULTS												
13				SONJ, UGB	375	350													
14				SONJ, UGB	350	325	ELPV, UGB	950	925										
15				SONJ, UGB	325	300	ELPV, UGB	925	900	SONJ, UGB	950	925							
16				SONJ, UGB	300	275	ELPV, UGB	900	875	SONJ, UGB	925	900							
17				SONJ, UGB	275	250	ELPV, UGB	875	850	SONJ, UGB	900	875							
18				SONJ, UGB	250	225	ELPV, UGB	850	825	SONJ, UGB	875	850							
19				SONJ, UGB	225	200	ELPV, UGB	825	800	SONJ, UGB	850	825							
20				SONJ, UGB	200	175	ELPV, UGB	800	775	SONJ, UGB	825	800							
21							ELPV, UGB	775	750	SONJ, UGB	800	775							
22							ELPV, UGB	750	725	SONJ, UGB	775	750							
23							ELPV, UGB	725	700	SONJ, UGB	750	725							
24							ELPV, UGB	700	675	SONJ, UGB	725	700							
25							ELPV, UGB	675	650	SONJ, UGB	700	675							
26							ELPV, UGB	650	625	SONJ, UGB	675	650							
27							ELPV, UGB	625	600	SONJ, UGB	650	625							
28							ELPV, UGB	600	575	SONJ, UGB	625	600							
29							ELPV, UGB	575	550	SONJ, UGB	600	575							
30										SONJ, UGB	575	550	PLOT-RESULTS						
31													ELPV, UGB	1500	1475	SONJ, UGB	1500	1475	
32													ELPV, UGB	1475	1450	SONJ, UGB	1475	1450	
33													ELPV, UGB	1450	1425	SONJ, UGB	1450	1425	
34													ELPV, UGB	1425	1400	SONJ, UGB	1425	1400	
35													ELPV, UGB	1400	1375	SONJ, UGB	1400	1375	
36													ELPV, UGB	1375	1350	SONJ, UGB	1375	1350	
37													ELPV, UGB	1350	1325	SONJ, UGB	1350	1325	
38													ELPV, UGB	1325	1300	SONJ, UGB	1325	1300	
39													ELPV, UGB	1300	1275	SONJ, UGB	1300	1275	
40													ELPV, UGB	1275	1250	SONJ, UGB	1275	1250	
41													ELPV, UGB	1250	1225	SONJ, UGB	1250	1225	
42													ELPV, UGB	1225	1200	SONJ, UGB	1225	1200	
43													ELPV, UGB	1200	1175	SONJ, UGB	1200	1175	
44													ELPV, UGB	1175	1150	SONJ, UGB	1175	1150	
45													ELPV, UGB	1150	1125	SONJ, UGB	1150	1125	
46													ELPV, UGB	1125	1100	SONJ, UGB	1125	1100	
47													ELPV, UGB	1100	1075	SONJ, UGB	1100	1075	
48													ELPV, UGB	1075	1050	SONJ, UGB	1075	1050	
49													ELPV, UGB	1050	1025	SONJ, UGB	1050	1025	
50													ELPV, UGB	1025	1000	SONJ, UGB	1025	1000	PLOT-RESULTS

Appendix 3. Mining order in scenario 1

----------Mining order in scenario 1!----------Mining order in scenario 1!----------

Phase	ELPV,current mine, UGB	Start Level	End Level	SONJ, current mine, UGB	Start Level	End Level	ELPV,Deep-I mine, SLC	Start Level	End Level	SONJ, Deep-I mine, SLC	Start Level	End Level	ELPV,Deep-II mine, SLC	Start Level	End Level	SONJ, Deep-II mine, SLC	Start Level	End Level	
1	Pillar	225	200																
2	ELPV, UGB	500	475																
3	ELPV, UGB	475	450																
4	ELPV, UGB	450	425																
5	ELPV, UGB	425	400																
6	ELPV, UGB	400	375	SONJ, UGB	550	525													
7	ELPV, UGB	375	350	SONJ, UGB	525	500													
8	ELPV, UGB	350	325	SONJ, UGB	500	475													
9	ELPV, UGB	325	300	SONJ, UGB	475	450													
10	ELPV, UGB	300	275	SONJ, UGB	450	425													
11				SONJ+Horizontal-pillar	425	400													
12	Horizontal-pillar	400	375	SONJ, UGB	400	375	PLOT-RESULTS												
13				SONJ, UGB	375	350	ELPV, SLC	550	575										
14				SONJ, UGB	350	325	ELPV, SLC	575	600										
15				SONJ, UGB	325	300	ELPV, SLC	600	625										
16				SONJ, UGB	300	275	ELPV, SLC	625	650										
17				SONJ, UGB	275	250	ELPV, SLC	650	675										
18				SONJ, UGB	250	225	ELPV, SLC	675	700										
19				SONJ, UGB	225	200	ELPV, SLC	700	725	SONJ, SLC	600	625							
20				SONJ, UGB	200	175	ELPV, SLC	725	750	SONJ, SLC	625	650							
21							ELPV, SLC	750	775	SONJ, SLC	650	675							
22							ELPV, SLC	775	800	SONJ, SLC	675	700							
23							ELPV, SLC	800	825	SONJ, SLC	700	725							
24							ELPV, SLC	825	850	SONJ, SLC	725	750							
25							ELPV, SLC	850	875	SONJ, SLC	750	775							
26							ELPV, SLC	875	900	SONJ, SLC	775	800							
27							ELPV, SLC	900	925	SONJ, SLC	800	825							
28							ELPV, SLC	925	950	SONJ, SLC	825	850							
29							ELPV, SLC	950	975	SONJ, SLC	850	875							
30							ELPV, SLC	975	1000	SONJ, SLC	875	900							
31										SONJ, SLC	900	925	ELPV, SLC	1000	1025				
32										SONJ, SLC	925	950	ELPV, SLC	1025	1050				
33										SONJ, SLC	950	975	ELPV, SLC	1050	1075				
34										SONJ, SLC	975	1000	ELPV, SLC	1075	1100	PLOT-RESULTS			
35													ELPV, SLC	1100	1125	SONJ, SLC	1000	1025	
36													ELPV, SLC	1125	1150	SONJ, SLC	1025	1050	
37													ELPV, SLC	1150	1175	SONJ, SLC	1050	1075	
38													ELPV, SLC	1175	1200	SONJ, SLC	1075	1100	
39													ELPV, SLC	1200	1225	SONJ, SLC	1100	1125	
40													ELPV, SLC	1225	1250	SONJ, SLC	1125	1150	
41													ELPV, SLC	1250	1275	SONJ, SLC	1150	1175	
42													ELPV, SLC	1275	1300	SONJ, SLC	1175	1200	
43													ELPV, SLC	1300	1325	SONJ, SLC	1200	1225	
44													ELPV, SLC	1325	1350	SONJ, SLC	1225	1250	
45													ELPV, SLC	1350	1375	SONJ, SLC	1250	1275	
46													ELPV, SLC	1375	1400	SONJ, SLC	1275	1300	
47													ELPV, SLC	1400	1425	SONJ, SLC	1300	1325	
48													ELPV, SLC	1425	1450	SONJ, SLC	1325	1350	
49													ELPV, SLC	1450	1475	SONJ, SLC	1350	1375	
50													ELPV, SLC	1475	1500	SONJ, SLC	1375	1400	
51																SONJ, SLC	1400	1425	
52																SONJ, SLC	1425	1450	
53																SONJ, SLC	1450	1475	
54																SONJ, SLC	1475	1500	PLOT-RESULTS

Appendix 4. Mining order in scenario 2

----------Mining order in scenario 2!----------																														
Phase	ELPV,current mine, UGB	Start Level	End Level	SONJ, current mine, UGB	Start Level	End Level	ELPV,Deep-I mine, UGB	Start Level	End Level	SONJ, Deep-I mine, UGB	Start Level	End Level	ELPV,Deep-I mine, SLC	Start Level	End Level	SONJ, Deep-I mine, SLC	Start Level	End Level	ELPV,Deep-II mine, SLC	Start Level	End Level	SONJ, Deep-II mine, SLC	Start Level	End Level	
1	Pillar	225	200																											
2	ELPV, UGB	500	475																											
3	ELPV, UGB	475	450																											
4	ELPV, UGB	450	425																											
5	ELPV, UGB	425	400																											
6	ELPV, UGB	400	375	SONJ, UGB	550	525																								
7	ELPV, UGB	375	350	SONJ, UGB	525	500																								
8	ELPV, UGB	350	325	SONJ, UGB	500	475																								
9	ELPV, UGB	325	300	SONJ, UGB	475	450																								
10	ELPV, UGB	300	275	SONJ, UGB	450	425																								
11				SONJ+Horizontal-pillar	425	400																								
12	Horizontal-pillar	400	375	SONJ, UGB	400	375	PLOT-RESULTS																							
13				SONJ, UGB	375	350	ELPV, UBG	950	925	SONJ, UGB	950	925																		
14				SONJ, UGB	350	325	ELPV, UBG	925	900	SONJ, UGB	925	900																		
15				SONJ, UGB	325	300	ELPV, UBG	900	875	SONJ, UGB	900	875	ELPV, SLC	550	575															
16				SONJ, UGB	300	275	ELPV, UBG	875	850	SONJ, UGB	875	850	ELPV, SLC	575	600															
17				SONJ, UGB	275	250	ELPV, UBG	850	825	SONJ, UGB	850	825	ELPV, SLC	600	625	SONJ, SLC	600	625												
18				SONJ, UGB	250	225							ELPV, SLC	625	650	SONJ, SLC	625	650												
19				SONJ, UGB	225	200							ELPV, SLC	650	675	SONJ, SLC	650	675												
20				SONJ, UGB	200	175							ELPV, SLC	675	700	SONJ, SLC	675	700												
21													ELPV, SLC	700	725	SONJ, SLC	700	725												
22													ELPV, SLC	725	750	SONJ, SLC	725	750												
23													ELPV, SLC	750	775	SONJ, SLC	750	775												
24													ELPV, SLC	775	800	SONJ, SLC	775	800												
25													ELPV, SLC	800	825	SONJ, SLC	800	825	PLOT-RESULTS										
26																			ELPV, SLC	1000	1025	SONJ, SLC	1000	1025					
27																			ELPV, SLC	1025	1050	SONJ, SLC	1025	1050					
28																			ELPV, SLC	1050	1075	SONJ, SLC	1050	1075					
29																			ELPV, SLC	1075	1100	SONJ, SLC	1075	1100					
30																			ELPV, SLC	1100	1125	SONJ, SLC	1100	1125					
31																			ELPV, SLC	1125	1150	SONJ, SLC	1125	1150					
32																			ELPV, SLC	1150	1175	SONJ, SLC	1150	1175					
33																			ELPV, SLC	1175	1200	SONJ, SLC	1175	1200					
34																			ELPV, SLC	1200	1225	SONJ, SLC	1200	1225					
35																			ELPV, SLC	1225	1250	SONJ, SLC	1225	1250					
36																			ELPV, SLC	1250	1275	SONJ, SLC	1250	1275					
37																			ELPV, SLC	1275	1300	SONJ, SLC	1275	1300					
38																			ELPV, SLC	1300	1325	SONJ, SLC	1300	1325					
39																			ELPV, SLC	1325	1350	SONJ, SLC	1325	1350					
40																			ELPV, SLC	1350	1375	SONJ, SLC	1350	1375					
41																			ELPV, SLC	1375	1400	SONJ, SLC	1375	1400					
42																			ELPV, SLC	1400	1425	SONJ, SLC	1400	1425					
43																			ELPV, SLC	1425	1450	SONJ, SLC	1425	1450					
44																			ELPV, SLC	1450	1475	SONJ, SLC	1450	1475					
45																			ELPV, SLC	1475	1500	SONJ, SLC	1475	1500	PLOT-RESULTS				

Appendix 5. Mining order in scenario 3

	----------Mining order in scenario 3!----------			----------Mining order in scenario 3!----------																											
Phase	ELPV,current mine, UGB	Start Level	End Level	SONJ, current mine, UGB	Start Level	End Level	EL,Deep-I mine, UGB	Start Level	End Level	PV,Deep-I mine, UGB	Start Level	End Level	SONJ, Deep-I mine, SLC	Start Level	End Level	EL,Deep-II mine, SLC	Start Level	End Level	PV,Deep-II mine, UGB	Start Level	End Level	SONJ, Deep-II mine, SLC	Start Level	End Level	
1	Pillar	225	200																							
2	ELPV, UGB	500	475																							
3	ELPV, UGB	475	450																							
4	ELPV, UGB	450	425																							
5	ELPV, UGB	425	400																							
6	ELPV, UGB	400	375	SONJ, UGB	550	525																				
7	ELPV, UGB	375	350	SONJ, UGB	525	500																				
8	ELPV, UGB	350	325	SONJ, UGB	500	475																				
9	ELPV, UGB	325	300	SONJ, UGB	475	450																				
10	ELPV, UGB	300	275	SONJ, UGB	450	425																				
11				SONJ+Horizontal-pillar	425	400																				
12	Horizontal-pillar	400	375	SONJ, UGB	400	375	PLOT-RESULTS																			
13				SONJ, UGB	375	350	EL, UGB	950	925	PV, SLC	550	575														
14				SONJ, UGB	350	325	EL, UGB	925	900	PV, SLC	575	600														
15				SONJ, UGB	325	300	EL, UGB	900	875	PV, SLC	600	625														
16				SONJ, UGB	300	275	EL, UGB	875	850	PV, SLC	625	650														
17				SONJ, UGB	275	250	EL, UGB	850	825	PV, SLC	650	675														
18				SONJ, UGB	250	225	EL, UGB	825	800	PV, SLC	675	700														
19				SONJ, UGB	225	200	EL, UGB	800	775	PV, SLC	700	725	SONJ, SLC	600	625											
20				SONJ, UGB	200	175	EL, UGB	775	750	PV, SLC	725	750	SONJ, SLC	625	650											
21							EL, UGB	750	725	PV, SLC	750	775	SONJ, SLC	650	675											
22							EL, UGB	725	700	PV, SLC	775	800	SONJ, SLC	675	700											
23							EL, UGB	700	675	PV, SLC	800	825	SONJ, SLC	700	725											
24							EL, UGB	675	650	PV, SLC	825	850	SONJ, SLC	725	750											
25							EL, UGB	650	625	PV, SLC	850	875	SONJ, SLC	750	775											
26							EL, UGB	625	600	PV, SLC	875	900	SONJ, SLC	775	800											
27							EL, UGB	600	575	PV, SLC	900	925	SONJ, SLC	800	825											
28							EL, UGB	575	550	PV, SLC	925	950	SONJ, SLC	825	850											
29										PV, SLC	950	975	SONJ, SLC	850	875	EL, SLC	1000	1025								
30										PV, SLC	975	1000	SONJ, SLC	875	900	EL, SLC	1025	1050								
31													SONJ, SLC	900	925	EL, SLC	1050	1075	PV, SLC	1000	1025					
32													SONJ, SLC	925	950	EL, SLC	1075	1100	PV, SLC	1025	1050					
33													SONJ, SLC	950	975	EL, SLC	1100	1125	PV, SLC	1050	1075					
34													SONJ, SLC	975	1000	EL, SLC	1125	1150	PV, SLC	1075	1100	PLOT-RESULTS				
35																EL, SLC	1150	1175	PV, SLC	1100	1125	SONJ, SLC	1000	1025		
36																EL, SLC	1175	1200	PV, SLC	1125	1150	SONJ, SLC	1025	1050		
37																EL, SLC	1200	1225	PV, SLC	1150	1175	SONJ, SLC	1050	1075		
38																EL, SLC	1225	1250	PV, SLC	1175	1200	SONJ, SLC	1075	1100		
39																EL, SLC	1250	1275	PV, SLC	1200	1225	SONJ, SLC	1100	1125		
40																EL, SLC	1275	1300	PV, SLC	1225	1250	SONJ, SLC	1125	1150		
41																EL, SLC	1300	1325	PV, SLC	1250	1275	SONJ, SLC	1150	1175		
42																EL, SLC	1325	1350	PV, SLC	1275	1300	SONJ, SLC	1175	1200		
43																EL, SLC	1350	1375	PV, SLC	1300	1325	SONJ, SLC	1200	1225		
44																EL, SLC	1375	1400	PV, SLC	1325	1350	SONJ, SLC	1225	1250		
45																EL, SLC	1400	1425	PV, SLC	1350	1375	SONJ, SLC	1250	1275		
46																EL, SLC	1425	1450	PV, SLC	1375	1400	SONJ, SLC	1275	1300		
47																EL, SLC	1450	1475	PV, SLC	1400	1425	SONJ, SLC	1300	1325		
48																EL, SLC	1475	1500	PV, SLC	1425	1450	SONJ, SLC	1325	1350		
49																			PV, SLC	1450	1475	SONJ, SLC	1350	1375		
50																			PV, SLC	1475	1500	SONJ, SLC	1375	1400		
51																						SONJ, SLC	1400	1425		
52																						SONJ, SLC	1425	1450		
53																						SONJ, SLC	1450	1475		
54																						SONJ, SLC	1475	1500	PLOT-RESULTS	